

REVIEW ARTICLE

Charge-coupled devices as particle tracking detectors

C. J. S. Damerell^{a)}

Rutherford Appleton Laboratory, Chilton, Didcot OX11 0QX, United Kingdom

(Received 15 September 1997; accepted for publication 12 December 1997)

Following a few years after the invention of the charge-coupled device (CCD) in 1970, the discovery of charmed particles established the need for very high precision (few μm) detectors for tracking high energy charged particles. This review describes the work which has evolved over the past 20 years from these disconnected events, both as regards the application of increasingly refined CCDs to particle tracking (in particular as vertex detectors for identifying heavy flavor quarks and tau leptons), and also the advances in CCD detector design stimulated by these requirements. The lessons learned in this work should provide guidance for the construction of large arrays of CCDs or active pixel devices in the future in a number of areas of science and technology. © 1998 American Institute of Physics. [S0034-6748(98)00104-X]

I. INTRODUCTION

There has been a long historical link between the technology of optical imaging and charged particle tracking detectors. Indeed, the adaptation of photographic film for this application (nuclear emulsions) provided tracking detectors for minimum-ionizing particles (hereafter referred to as MIPs), with few μm precision.¹ Such detectors have had an illustrious history in particle physics; for example, they were used exactly 50 years ago in the first observation of the decay of pi to mu mesons.²

Over the years, the technologies of optical imaging (still largely based on photographic film) and particle tracking (increasingly using electronic detectors such as spark chambers and multiwire gaseous chambers) drifted apart. However, the invention of the charge-coupled device (CCD) in 1970^{3,4} started a revolution which is still having profound effects in the fields of optical imaging, particle tracking, x-ray detection, analog storage devices, etc. Once again, one is dealing with a technology with multidisciplinary applications, with consequential benefits as ideas generated from one application area find uses in others. However, at the time of its invention, the potential value for particle tracking went unrecognized. The emphasis in particle physics was for ever larger area coverage (tens of square meters) and the typical drift chamber precision of $\sim 100 \mu\text{m}$ was believed adequate for all applications.⁵

The discovery of charm, tau leptons, and beauty/bottom particles during the period 1974–1977 (particles with lifetimes in the range 10^{-13} – 10^{-12} s) profoundly changed the picture. Suddenly it was seen to be important to achieve micron-level tracking precision in small detectors close to the interaction point in order to recognize events containing heavy flavor particles, and ideally to reconstruct the trees of

vertices, primary, secondary and possibly tertiary (PV, SV, TV), assigning the tracks unambiguously to their true parent vertices. In Fig. 1 is a sketch of the typical topological information contained in high energy jets of particles that result from the production of heavy quarks, and the possibility of extracting this information with the aid of two or more layers of high precision tracking detectors near the interaction point (IP). Each jet of particles in this example includes one containing a b quark, whose decay (SV) releases a charm particle which subsequently decays (TV). While Fig. 1 shows a two-layer detector, in practice at least three layers would be desirable in order to provide redundancy and an internal alignment capability.

What technology could be used for such high-precision detectors? Nuclear emulsions made a partial comeback, but their lack of electronic readout and their inability to selectively register triggered events were major handicaps. Major efforts were made to improve the precision of the then-popular tracking detectors (bubble chambers, multiwire drift chambers, etc.) but with only limited success. These techniques were fundamentally unable to meet the challenge of the “new physics.”

The way forward was shown to lie with silicon detectors. Germanium and silicon detectors (in the form of reverse-biased diodes with extensive depletion regions) had been used for the detection of ionizing radiation for over 30 years.⁶ Even as position sensitive detectors for particle tracking, albeit with spatial resolution of ~ 1 mm, silicon strip devices were already in use as beam hodoscopes, etc. The development of high-precision microelectronic fabrication techniques, the “planar process,” lent itself perfectly to the production of microstrip detectors with $\sim 5 \mu\text{m}$ tracking precision for MIPs.⁷ A very readable account of the remarkable human stories associated with the development of microelectronics is to be found in George Gilder’s book on the subject.⁸ While the development of silicon microstrip detec-

^{a)}Electronic mail: c.damerell@rl.ac.uk

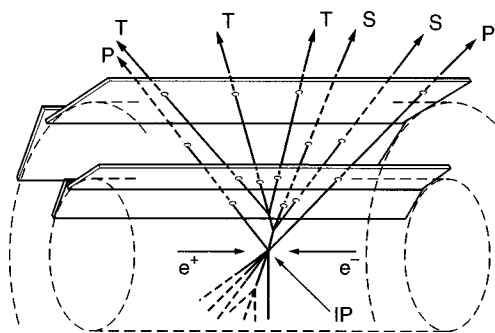


FIG. 1. Sketch showing the principle of a two-layer pixel-based vertex detector for reconstructing the topology (PV, SV, TV) of a b jet. Tracks are labeled according to their parent vertices.

tors was being pioneered by the CERN-Munich part of the ACCMOR collaboration at CERN, the RAL part of the same collaboration initiated the development of CCD particle tracking detectors.⁹ It was quickly demonstrated that such detectors could perform with similar precision to silicon microstrip detectors¹⁰ but (being pixel based rather than using strips) they had the further advantage of providing true space-point information. As such, they could be placed much closer to the IP with no significant problems of track merging. In contrast to these advantages, CCDs lack the fast timing capability (strobed coincidence logic) of microstrip detectors with independent readout electronics on every strip. In the ACCMOR experiment NA32, a pair of CCD detectors followed by six planes of microstrip detectors formed a powerful combination, allowing the determination of the shortest charm particle lifetimes ever to be measured.¹¹ Over the ensuing decade, microstrip detectors have found the more widespread applications, particularly for general purpose b -quark tagging. However, CCD detectors have continued to provide state-of-art vertex detection where experimental conditions were appropriate. Microstrip detectors, being projective devices, are limited to environments with a relatively low density of hits, while CCD detectors, being pixel based, can accommodate far higher hit densities. While microstrip detectors, used mainly as particle physics tracking detectors, are dependent on scientific users, CCDs, being suited to the recording of two-dimensional (2D) information such as optical images, have an enormous user base, including domestic still and video cameras, medical and dental x-ray applications, astronomy (visible light and x rays), synchrotron radiation, etc. Without this broad market, such complex devices would never have been developed for the small particle tracking/vertex detector community. While the assembled detectors used in this field are among the largest of any CCD-based instruments (up to 100 CCDs and 300 Mpixels), the overall market provided by particle physics is relatively minute. However, due to the demanding technical requirements in this field, the particle tracking application is of considerable interest to manufacturers of scientific CCDs. The efforts to satisfy these requirements have raised the understanding and thereafter the quality of the devices to the benefit of all classes of scientific users.

In contrast with the symbiosis between the different scientific application areas, it should be pointed out that the

overlap between the domestic and scientific CCD manufacturers is almost nonexistent. The reason for this is partly the fact that the domestic device manufacturers are understandably focused on the huge, highly competitive, mass markets; they have no time to deal with "nonstandard" requirements. Furthermore, their entire design base is locked into extremely shallow active layers (in order to achieve sharp images even in the red region of the spectrum). As such, many of their device characteristics are opposed to those sought by particle tracking and x-ray detection users. The needs of scientific customers have been filled by highly specialized companies set up for the production of specially designed CCDs in small volume, with full flexibility to adapt the designs for each specific application area. In one or two cases, research laboratories in which CCDs are heavily used have developed their own integrated circuit processing capabilities to the level where they are able to produce their own devices in house, but for the most part users have found it preferable to do the design in conjunction with a commercial manufacturer having a sufficient overall customer base to maintain the extremely costly state-of-the-art processing facilities. In fact even the best equipped manufacturers of CCDs for the scientific community are lagging behind the state of the art in feature sizes, etc, when compared with the largest manufacturers of computer memory chips, CCDs for domestic consumer products, etc. This will always tend to be the case, given the relative sizes of these markets. Nevertheless, by comparison with silicon microstrip detectors, the market for scientific CCDs is relatively large and multidisciplinary, and the production facilities are highly sophisticated. Thanks to this fortunate state of affairs, the particle tracking/vertex detector community has access to devices whose complexity far outstrips the home grown in-house detectors which formerly characterized high energy physics experiments. Furthermore, the sophistication of available devices is evolving rapidly, carried along by the ongoing pace of developments in the planar technology of microelectronics.

II. CCD TRACKING DETECTORS: OPERATING PRINCIPLES AND PERFORMANCE

A. MIP signals in thin silicon detectors

The advantages of solid state detectors for high-precision particle tracking have been vividly apparent since the days of nuclear emulsions. Electrons released by the ionization process are confined extremely closely to the particle trajectory. Silicon has the further advantage that, due to its small band gap (1.1 eV), MIPs generate prolific signals (~ 80 electron-hole pairs per μm of track length). Since (as we shall see in Sec. II D) the CCD output signal processing permits noise levels below $100 e^-$; a detector thickness of $10\text{--}20 \mu\text{m}$ is sufficient to achieve MIP detection with excellent signal-to-noise performance. This minimum detector thickness is far less than with other technologies (e.g., silicon microstrip detectors) and carries with it several distinct advantages:

- (1) reduced probability of ejecting δ electrons of range sufficient to spoil a coordinate measurement;

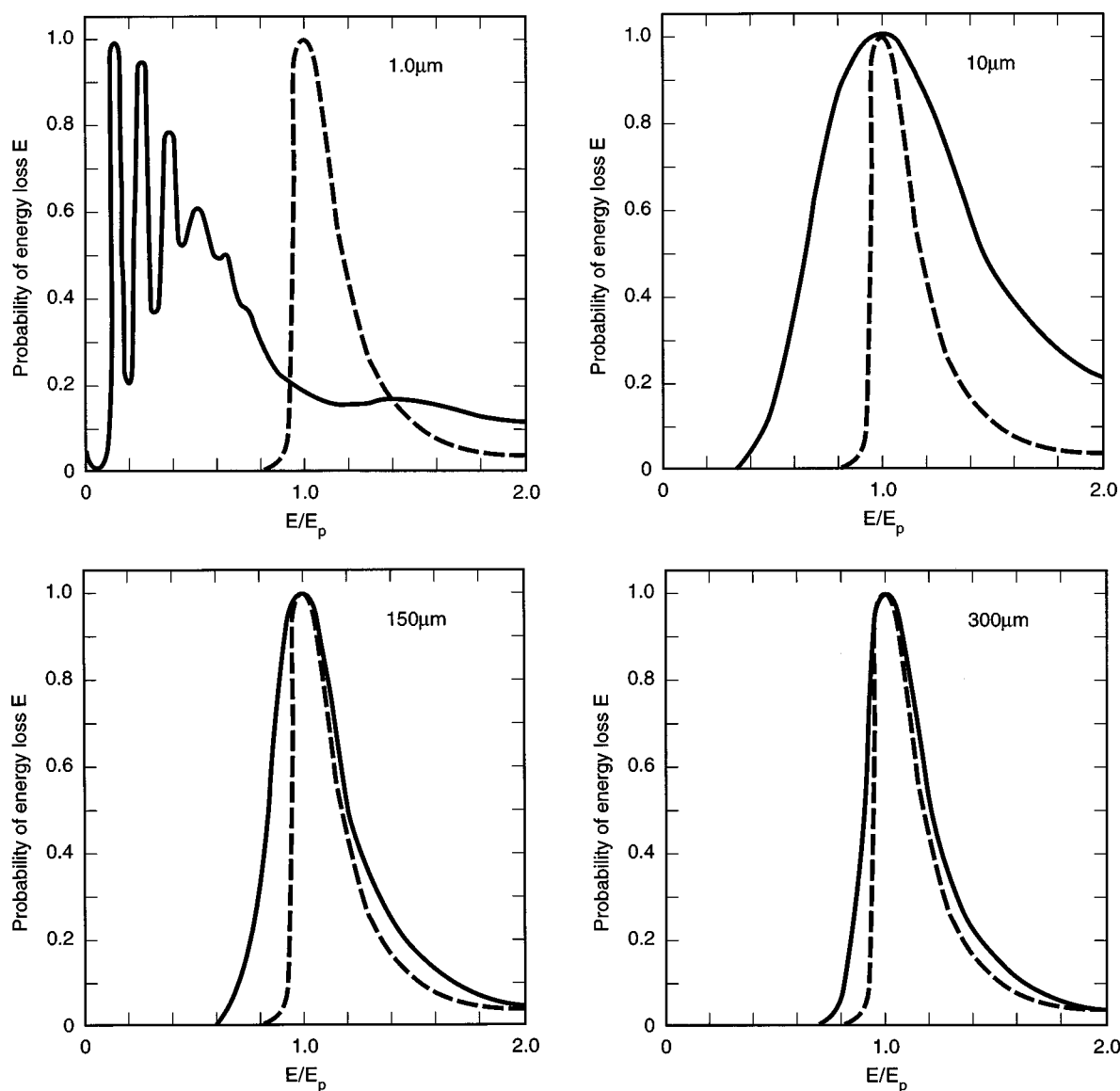


FIG. 2. Energy loss distributions for various thicknesses of silicon detector with (in each case) a Landau distribution for comparison. The separate peaks corresponding to 0, 1, 2... plasmon excitation are already merged by a thickness of 10 μm .

- (2) reduced projected track length for oblique incidence (in thick detectors the precision for oblique tracks is seriously degraded);
- (3) the opportunity to thin the entire detector down to the active layer thickness if desired (thinning may be extremely important in reducing multiple scattering).

Around 1980, when CCDs were first considered for MIP detection, it was far from clear whether this would be possible even in principle, with high efficiency. The quantity W (the mean energy for electron-hole pair creation, ~ 3.7 eV) was of course well known; what was far from clear was the expected fluctuations (straggling) in the energy deposition by a MIP for such thin samples. Theoretical estimates varied widely, and some calculated distributions were so broad that high efficiency MIP detection would have been ruled out. Fortunately the measurements¹⁰ for ~ 20 μm detector thickness demonstrated that the more optimistic earlier estimates¹² had been correct. There followed papers^{13,14} making detailed comparisons between refined theoretical

procedures and the new data, and finally a definitive review paper¹⁵ which provided the full description of the energy loss of charged particles in solid silicon. What emerged from these calculations was that the straggling spectra, while narrower than some early estimates, are much broader than the widely used Landau distribution, the discrepancy becoming greater for thinner detectors. For very thin samples (e.g., 1 μm) the energy loss is typically characterized by the excitation of a small number of plasmons for M -shell electrons (with mean plasmon energy 16.7 eV). Such cases are best simulated by Monte Carlo calculations;¹⁶ results for a range of detector thicknesses are plotted in Fig. 2.

It should be noted that what the detector physicist measures is not the energy loss, but the charge released in the detector. These are related by W , with a statistical factor F (the Fano factor) which expresses the suppression in the fluctuations in the number of pairs created below that which would be given by Poisson statistics. There has been much recent experimental¹⁷ and theoretical¹⁸ work on W and F for

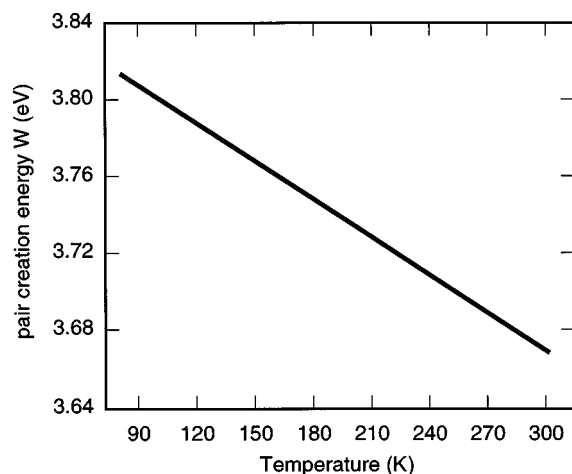


FIG. 3. Temperature dependence of the pair-creation energy W in silicon. A detector operated cold will produce slightly smaller MIP signals than one at room temperature.

silicon. It is sufficient here to note that for the thin detectors we are concerned with, the conversion to charge released leads to a negligible further broadening with respect to the energy loss distributions shown in Fig. 2. It should however be remembered that the precise value of W depends weakly on the temperature (see Fig. 3), reflecting the temperature dependence on the silicon band gap.

B. CCD operating principles and general performance

Having just discussed the advantages of silicon as a precision tracking medium, it should now be pointed out that an even more compelling factor in the choice of this material for detectors has been the development of the planar process for integrated circuits (ICs). This has allowed the production of a huge variety of detectors bonded to, or combined on, the same wafer with sophisticated readout ICs. CCDs form some of the most advanced of the second class of detectors. Their unique advantage for tracking lies in their ability to confine the signal charge within an extremely compact collection volume, and then to transfer the signal packet without loss onto the gate of a very low capacitance on-chip sensing transistor. Despite these attractions, this on-detector multiplexing has its disadvantages; the serial sensing of the signals from a large number of pixels by a single output circuit takes time. CCDs are correctly seen as “slow” detectors by comparison with those where the signals are sensed in parallel by a separate output circuit for every detector element. In this review, we focus on various particle tracking applications for which CCD detectors have proven their superiority; these are areas in which the above attributes are particularly important, and where special procedures have been devised to allow the requirements of long readout time to be accommodated.

Let us now understand how the very thin active layers referred to in Sec. II A can be achieved. A CCD consists globally of a reverse-biased structure (usually n^+ on a p -type substrate), on which a metal–oxide–semiconductor (MOS) gate structure and other features are superimposed. Figure 4 shows the cross section of a typical device. It consists of a lightly doped epitaxial p layer on a heavily doped

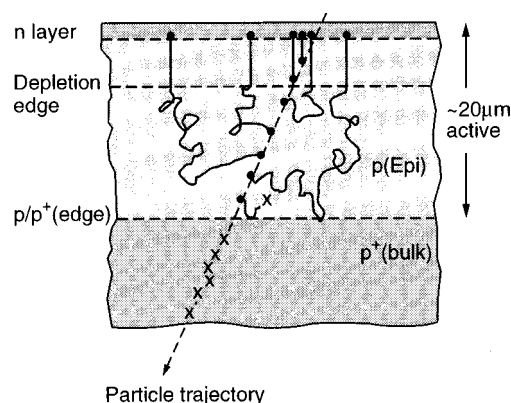


FIG. 4. Charge collection within a buried-channel CCD structure.

p^+ substrate, with the top $\sim 1 \mu\text{m}$ of the p layer doped by ion implantation of phosphorus, followed by thermal activation, to become n^+ . The partial depletion of the n^+/p region creates a potential minimum for storage of charge carriers (electrons in this case) just above the depth of the n^+/p edge, into which signal electrons generated within the depletion region of thickness $\sim 5 \mu\text{m}$ will be transported by drift in the electric field. But this is not the full story. Minority carriers (electrons) generated in the undepleted p -type substrate will diffuse isotropically. Those which reach the depletion edge will be drawn into the potential energy minimum. However, those which diffuse to the p/p^+ edge feel a potential barrier due to the thin intrinsic depletion layer; this acts as a perfect reflector, so even these electrons continue to diffuse and rapidly find their way into the storage region. Reference 19 is possibly the first paper in which the principles of this general phenomenon were explicitly described.

The localization and transfer of this stored signal charge is achieved by means of two structures, an imaging area (I) and an adjacent readout register (R), sketched in Fig. 5. Charge is confined in depth by the potential distribution

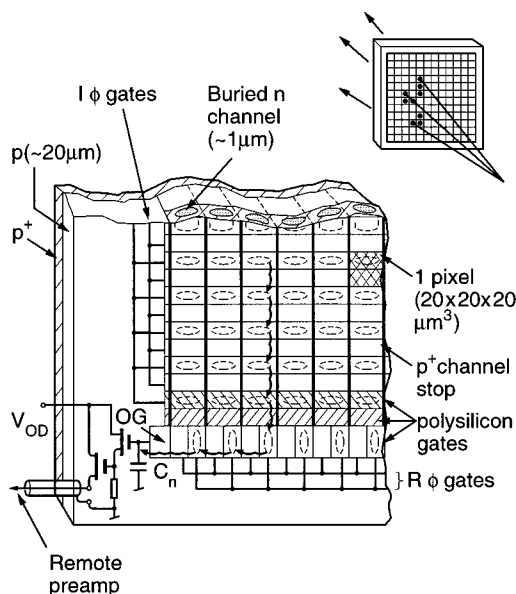


FIG. 5. Upper right: Sketch of charge storage in a CCD detector traversed by a number of ionizing particles. Lower left: Corner region of the CCD showing the principal structural features.

mentioned above. Transversely, charge confinement in the imaging area is by means of vertical p^+ implants (channel stop regions) and horizontal polysilicon gates, electrically isolated from each other and from the substrate. By manipulating the potentials on these $I\phi$ gates, charge is transferred in parallel down each column towards the output register, in such a way that the 2D image is preserved. On each I shift, the charge from the bottom row of the image area is transferred into the R register. Then there is a pause of vertical transfer in order to allow this row to be read out serially through the output circuit at the end of the R register, after which the next row transfer is made. The horizontal transfer along the R register is achieved by a similar, independent set of $R\phi$ gates. With each horizontal transfer, the signal charge from the first pixel in the R register is transferred onto the output node, a diode implant which is directly connected to the gate of an adjacent MOS field effect transistor (MOSFET). The resultant modulation of the drain current in the FET is used to sense the signal associated with that pixel.

CCDs used for typical optical imaging are supplied with signals of order $10^5 e^-$ per pixel. The reduction by a factor of ~ 100 in CCDs used for particle tracking detectors imposes two major challenges on the CCD design and operation. First, there is the requirement of extremely efficient, noiseless transport of the tiny charge packet through possibly thousands of transfers within the imaging and readout regions of the device. This is discussed in detail in Sec. II C. The second major challenge is the electronic noise performance of the output circuit and associated signal processing; this is discussed in Sec. II D. There is a third challenge imposed on CCDs used for particle tracking; they are always operated in a radiation environment. This implies that having found solutions to the first two critical requirements, care has to be taken to ensure that these are not destroyed by the operating environment. This is discussed in Sec. V.

For clarity, what has been described in this section, and what will be in the remainder of this review, is one particular class of CCD architectures that has proved to be the most generally useful for particle tracking. It should however be pointed out that there are numerous other options, some of which might be of interest in future, for example, as the experimental requirements are changed. Examples of available options are:

- (1) signal storage: electrons (n channel) or holes (p channel);
- (2) signal storage: buried channel (BC) or surface channel (SC);
- (3) substrate material: epitaxial or bulk (and in each case, of what resistivity?);
- (4) phases per pixel: options range from 1 (virtual phase) to 4;
- (5) "pinned" operation for reduced dark current;
- (6) charge sensing other than the "floating diffusion" system (see Sec. VI A).

The reader interested in exploring these options is referred to the extensive literature on the subject. References 20–22 are books which provide comprehensive discussions, Ref. 23 includes a pedagogical description of CCD designs

for particle tracking. As well as the papers of Refs. 3 and 4 describing the invention of the device, important discussions of subsequent developments are to be found in Refs. 24 and 25 (invention of the buried-channel architecture),²⁶ (charge distribution in buried-channel devices),²⁷ (general review),²⁸ (first use of epitaxial material),²⁹ ("pinned" operation),³⁰ (integration of high and low resistivity regions on the same wafer),³¹ (review of performance limitations)³² (numerous novel architectures), and³³ (ideas for extending performance limits). As well as providing a record of the extraordinary developments that have taken place since the original CCD prototype (a six pixel linear device in which 1% of the signal charge was lost in each transfer), these papers provide possibly valuable lessons for the future. For example, the first attempts to build CCDs on epitaxial material were widely predicted to fail due to the poorer crystalline quality than bulk silicon. In fact they worked much better due to the intrinsic gettering of impurities into the oxygen-rich substrate. Also, the papers in Ref. 32 were largely motivated by the tremendous interest in extending the performance of optical CCD imagers to high definition television (HDTV) applications. While it remains true (as mentioned in Sec. I) that the manufacturers concerned are not interested in the small "scientific" market, their extraordinary R&D programs may well provide ideas that are applicable to this market.

A pioneering paper on the applications of CCDs to low signal levels³⁴ includes the invention of a method of signal processing called correlated double sampling (CDS) which will be discussed in Sec. II D.

The use of CCDs for particle tracking is closely allied to x-ray detection. In fact, x rays provide a valuable tool for device characterization, since they deposit their signals in very compact clusters, allowing charge collection from the different regions of the CCD (Fig. 4) to be explored separately. Useful papers from the x-ray community (which provide pointers to many others) are to be found in Refs. 35–38.

C. Charge transfer efficiency

Large area CCDs are the key to state-of-the-art particle tracking detectors. However, this implies phenomenally high charge transfer efficiencies (CTEs) as the signal packet is shifted from pixel to pixel. (Note also the term charge transfer inefficiency; $CTI = 1 - CTE$.) With modern devices, values of charge transfer inefficiency (CTI) $< 10^{-5}$ are achieved, compared with $\sim 10^{-2}$ with the original designs. This improvement by three orders of magnitude is the result of great ingenuity and hard work by many people.

In considering the factors leading to imperfect charge transfer, one should distinguish between signal electrons which are free and those which are trapped. For free electrons, charge motion on the manipulation of gate electrodes is in general due to a combination of thermal diffusion, self-induced drift and fringing field drift. In the case of small charge packets such as one is concerned with in MIP detection, only the third of these is important. For gate dimensions $7\text{--}10\text{ }\mu\text{m}$ typical of three or two phase CCDs with $20\text{ }\mu\text{m}^2$ pixels, fringing field drift can provide $CTE \geq 99.999\%$ at clock frequencies up to $\sim 100\text{ MHz}$. High speed operation is

dependent on strong fringing fields, which provided one of the original motivations for moving from the surface-channel to buried-channel architecture, under the name peristaltic CCD.³⁹ (Note also the term bulk channel, which is again synonymous with buried channel.)

Regarding charge trapping, transfer inefficiency results from atomic impurities, crystal defects, etc. within the storage volume, which trap electrons from the signal packet for a sufficiently long time that they are lost from their parent packet as this is transferred along the CCD register. Again, the early surface-channel devices were particularly subject to such losses, as the electrons of the signal packet interacted with the continuum of "interface states" at the Si/SiO₂ interface. These give rise to energy levels that populate the entire band gap and can trap electrons with a huge range of trapping time constraints. Switching to buried-channel devices greatly reduced this problem, although one was then dependent on the bulk properties of the material. Due to impurities in the starting material and/or those introduced in processing, bulk trapping in early CCDs was often serious. Positively charged traps can have "giant" cross sections for capturing signal electrons;⁴⁰ gold was a particularly dangerous impurity. Trap-induced CTI is at its worst for small signal packets, since in such cases the storage volume will be constant (being defined by the electron thermal energy and the shape of the potential well) whereas for large signal packets the charge density will be constant (given by the concentration of charged donors in the *n* channel).

Trap densities in modern CCDs have been reduced to extremely low levels so that, even for small packets of a few hundred electrons, CTE $\geq 99.999\%$ is attainable under favorable operating conditions. The quantitative discussion of charge trapping is deferred to Sec. V, since in practice the only traps that pose serious problems in well designed and fabricated modern tracking detectors are those induced by radiation damage.

The progress to the present state of excellence is recorded in a number of important papers. Charge transfer for free electrons was first considered in Refs. 41 and 42, in the context of surface-channel devices. In Ref. 43 the effect of bulk traps in buried-channel CCDs was considered theoretically, and experimental techniques for CTE measurement were established which are still used. The theoretical treatment in terms of the Shockley–Hall–Read generation–recombination theory^{44,45} (SRH theory), is taken up in Sec. V. The potentially disastrous effect of interelectrode gaps was treated in Ref. 46, and the vital role of temperature (both as a diagnostic aid and in determining the optimal operating conditions) regarding bulk traps was discussed in Ref. 47. The specific case of CTE at low signal levels was discussed in Ref. 48, and the effects of carrier freeze out, which increase dramatically below 90 K, were discussed in Ref. 49. An important study of the theoretical modeling of CTE in buried-channel CCDs at low temperature is found in Ref. 50; the dependence on pixel clocking rate is treated in Ref. 51.

As well as effects related to free charge transport and signal trapping, there is a third class of effect which can degrade CTE in unirradiated devices. Due to design or processing defects, there may exist potential wells (also called

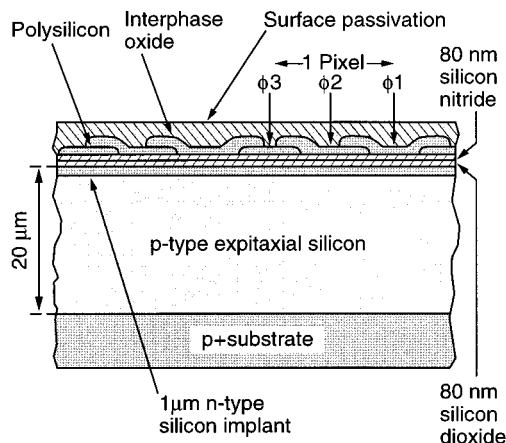


FIG. 6. Gate structure of a modern three-phase CCD register designed to avoid potential wells due to radiation-induced charge buildup or other spurious charge in the dielectric or surface-passivation layers.

potential pockets in the literature) within or between gates, which can act to inhibit complete charge transfer; their effect can be particularly severe (even catastrophic) for small signal charge packets.

One most important lesson has been the great importance of defining the buried-channel potential over the full sensitive area of the device. This is achieved by carefully processing the gates to ensure full overlap at the edges (see Fig. 6). However, excessive gate overlap increases the capacitance to be driven, and hence worsens the clock feedthrough problem. By using modern processing equipment and procedures, it is possible to achieve $\sim 2 \mu\text{m}$ gate overlaps safely.

The importance of finite overlaps, and the need to check thoroughly that these have been achieved over the entire area of each production device, is illustrated by a problem that arose in testing large CCDs for the SLD upgrade vertex detector. The device quality control (QC) included illumination with $\sim 4 \times 10^6$ x rays from an ⁵⁵Fe source (this yields the Mn *K*α line with energy 5.9 keV, generating $\sim 1600 e^-$ signal clusters). Looking along every column of the CCD separately and setting a threshold a little below the *K*α peak, the hit rate versus *I* address could be studied. For a well behaved CCD column the rate would vary slowly over the range *I* = 0 at the R register to *I* = 2000 at the remote end of the image area. In some cases (see Fig. 7) one would observe an abrupt fall in hit rate at some *I* address, and this would usually affect only one column; the neighbors would be perfect. The problem went undiagnosed for a while, until a particularly bad batch exhibited blockage of several adjacent columns at the same *I* address. Microscopic examination of the area revealed the cause. Due to localized overetching, the nominal overlap between gates was transformed in these areas into a ragged gap, as seen in Fig. 8. Such a feature would then expose the buried channel to fixed charges in the gate oxide, interface oxide, or polyimide passivation. This charge could of course create a local disturbance to the channel potential, sufficient to block or trap small signals. The fact that CCDs normally work so well in terms of charge transfer of signals as small as a few electrons is due, not to some near-magical uniformity of the channel potential, but to the

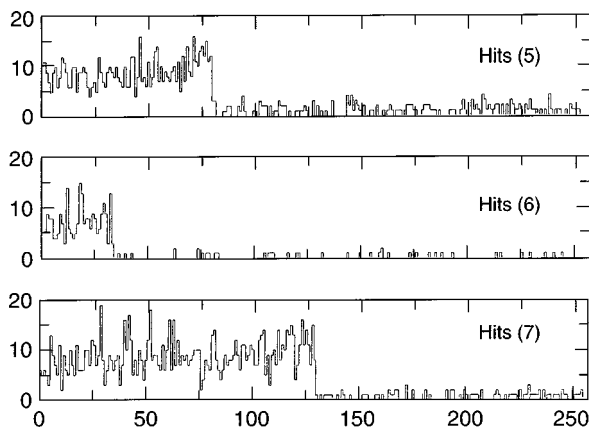


FIG. 7. Hit rate as a function of the I address along a few columns having significant traps. The trap location can be precisely determined by the sharp fall in hit rate.

Poole–Frenkel effect⁵² which (through quantum mechanical tunneling) effectively drags electrons out of small irregularities between the gates of either the imaging or readout register. It is in fact quite reassuring to observe the scale of device imperfections that do cause problems for small-signal operation; such processing faults can certainly be addressed and largely eliminated. There will inevitably be much smaller potential variations (e.g., due to slight fluctuations in the thickness of the gate oxide) on all devices, but these are evidently well below the threshold required to cause any CTE loss.

Such experiences demonstrate the importance of high statistics test data in establishing the performance of these devices for particle tracking. CCDs provide data of unprec-

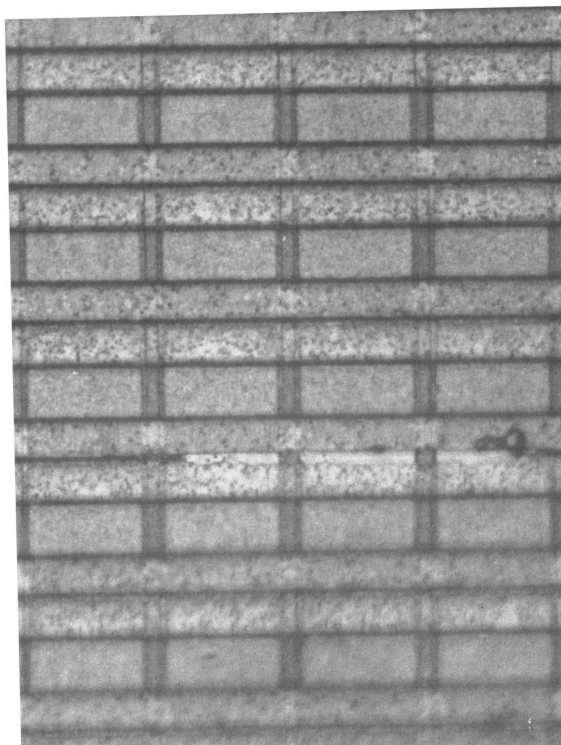


FIG. 8. Photomicrograph of the CCD imaging area in a region of high trap density. The ragged gate edge due to overetching is clearly visible.

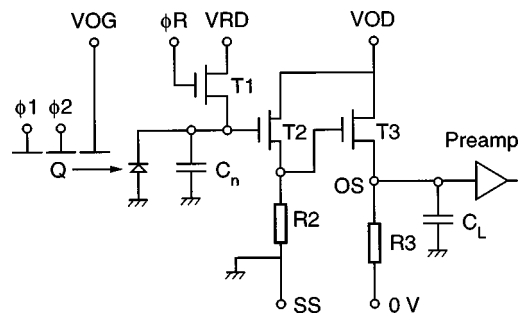


FIG. 9. Schematic diagram of a two-stage output circuit.

edented granularity for an electronic detector (comparable to nuclear emulsions, and in some ways superior, e.g. as regards spatial precision), but this granularity carries with it the potential for microscopic defects which can cause localized performance problems. For the most part, it is not however necessary to study intensively each pixel. Being read out in a column-based architecture, studies of the behavior along the length of each column generally suffice to uncover significant problems.

D. Output signal processing

The aim with any tracking detector will be to achieve a single layer efficiency $\geq 99\%$. This is particularly the case for a vertex detector, since the measurement from the innermost layer is especially valuable and, if lost, cannot be fully recovered by the outer tracking, due to multiple scattering effects.

Achieving such a MIP efficiency with a $20\ \mu\text{m}$ active layer thickness is a significant challenge. Measurement of the mean signal ($\sim 1600\ e^-$) would be quite straightforward, but as discussed in Sec. II A, this is considerably broadened by straggling, on top of which a MIP cluster is typically divided between three or four pixels, even for tracks with normal incidence to the CCD surface.

Assuming the CTE complexities discussed in the previous sections are under control, one may take as a starting point the noiseless, lossless transfer of the originally collected pixel signal charge to the output node of the CCD. The function of the output circuit is to convert this charge to a voltage that can be digitized in the front-end off-CCD electronics. In tracking detectors, the requirements for noise performance are (by the standards of scientific CCDs) modest ($\leq 100\ e^-$ rms, whereas astronomers require $< 10\ e^-$), but the readout needs to be fast (R register clocking rates in the region 10–100 MHz). These atypical requirements create some complications but make it possible to bypass others.

Nearly all currently used charge sensing circuits are of the “floating diffusion” type, shown in Fig. 9. The circuit comprises an output gate, an output diode for charge collection, a reset transistor T1, and an output transistor T2 operated as a source follower. Conventionally, the “output node” (output diode plus T2 gate) is reset to a reference voltage V_{RD} by pulsing T1 into conduction prior to each transfer of signal charge. The change in the node voltage on signal charge transfer, sensed by the source follower, then provides a measure of the charge. This is repeated for each

pixel in the array. Johnson (and other) noise in the circuit leads to random fluctuations in the output voltage, and thereby sets a limit on the minimal detectable signal.

A major potential noise source arises from "reset noise," fluctuations in the voltage on the output node when the reset transistor is turned off. In magnitude this amounts to

$$\left(\frac{kT}{C_n}\right)^{1/2} \text{ rms V,}$$

where C_n is the node capacitance, and can amount to $>100 e^-$, which would be quite unacceptable. This noise source is conventionally eliminated by the technique of correlated double sampling (CDS),^{34,53} which essentially consists of measuring the voltage level before and after each transfer, and recording the difference. This is intrinsically slow, and can be avoided completely in particle tracking detectors, where the data density is always so sparse that one can integrate the signal charge from the entire R register, resetting the node only at the end of each row. The signal in any pixel is then simply the voltage difference between the sample for that pixel and its predecessor.

The second (and now unavoidable) noise source is that associated with the drain current flowing in transistor T2, which generally has both white and $1/f$ components. As will be referenced at the end of this section, much progress has been made in optimizing the MOSFET design to minimize the $1/f$ and other undesirable noise sources (e.g., due to hot electrons creating avalanche current near the drain in devices operated in saturation). For tracking systems, the problem is again simplified. Modern on-CCD FETs have $1/f$ noise corner frequency <200 kHz, so at the readout rates we are concerned with, only the white noise floor due to the Johnson noise in the FET channel resistance is important.

The CCD node capacitance C_n can be divided into two components, C_d the detector capacitance and C_g the FET gate capacitance. The FET is usually designed to minimize the equivalent noise charge (ENC) which implies making $C_g = C_d$; see Ref. 33. This is an example of a completely general noise optimization theorem, as discussed in Ref. 54. Putting in typical experimental values for FET performance parameters from Ref. 33, the rms noise associated with the output transistor, in the case where the signal is integrated through the interpixel period, with a pixel clocking frequency of f_c MHz, is given by $\text{ENC} \approx 0.91 f_c^{1/2} C_n^{1/2} e^-$, where C_n is in fF. Below ~ 5 MHz, this formula becomes increasingly inaccurate as the $1/f$ noise becomes significant.

The procedure for noise minimization is thus primarily to reduce C_n . Vast progress has been made in this area, with values of 25 fF being currently available and 10 fF ultimately possible. For a readout frequency of 50 MHz, the former value would give $\text{ENC} = 32 e^-$ rms, more than adequate for MIP detection with full efficiency.

However, the ongoing reduction in detector capacitance matched by the output FET capacitance (by reducing the channel width W_F) carries with it a serious penalty; the output impedance is proportional to $1/W_F$. In order to achieve the required bandwidth for high sample rates, the load capacitance must be correspondingly reduced. This problem

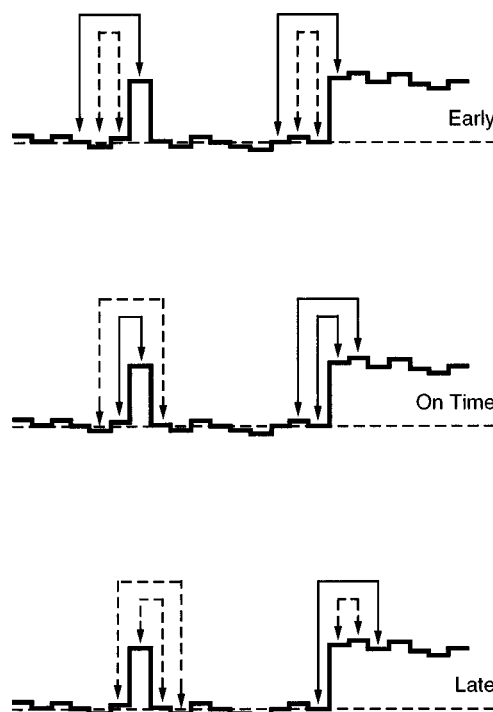


FIG. 10. Extended row filter operating on a row of CCD digitized data. Whereas both overlapping samples register a hit when "on time" for valid data, this never happens for the pickup/noise spike.

has been solved by integrating a second stage on-chip source follower as shown in Fig. 9, with transistor T3 having a channel width approximately 10 times that of T2, and hence with a sufficiently low impedance to drive the load capacitance connecting to the front-end amplifier.

The procedure of resetting the node only at the end of each row has permitted an important noise-suppression feature, called extended-row filtering (ERF),⁵⁵ which can be understood by reference to Fig. 10. The principle is that whereas a valid signal creates a step in the node voltage, pickup spikes or rare (many standard deviation) noise fluctuations will normally be restricted to one sample. The complete row of data is digitized on the front-end electronics board, and the signal associated with each pixel is taken to be the minimum of two overlapping samples as shown in Fig. 10. These two samples will be closely similar for valid data, but one of them will be ~ 0 (and hence cause the global estimate to be discarded as below threshold) in the case of noise. This procedure has recently been further refined⁵⁶ leading to extremely low noise rates even from a detector system of >300 Mpixels.

Key papers in the long evolution to the present spectacular noise performance of CCDs that should be consulted for much more detailed discussions include Ref. 57, a pioneering review of all CCD noise sources. References 58 and 59 established the advantage of the buried channel as opposed to the surface-channel MOSFET as regards $1/f$ noise, including the limits of V_{DS} and I_D necessary if that advantage is to be maintained. Valuable general reviews of the performance limitations in CCDs, especially as regards output circuit noise, are Refs. 31 and 33. In general, while much of the literature is related to noise optimization for applications

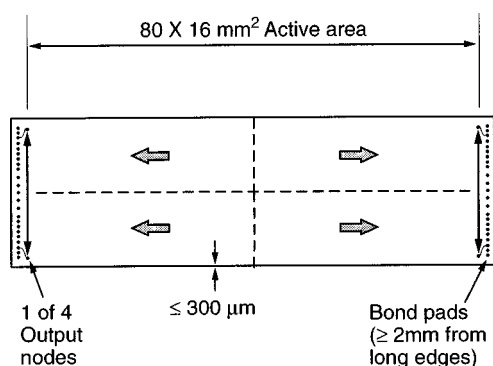


FIG. 11. Basic architecture of a modern particle-tracking CCD. The parallel register (I register) shifts signal packets to each end of the device. A serial register (R register) at each end shifts signal packets to a pair of output circuits.

such as astronomy where the requirements are rather different, the progress made has frequently been directly applicable in extending by a factor of 200 the frequency range over which one can meet the noise requirements for MIP tracking detectors. The first efficient MIP detection was achieved at an R clocking frequency of 50 kHz. Similar noise performance can now be achieved at 10 MHz.

E. Device architectures

The simple postage stamp sized CCDs with single output, as sketched in Fig. 5, have long been superseded by more advanced architectures. Figure 11 shows a recent example of particular interest for tracking. It is 10 times larger than early devices (ideal for constructing a large area detector) but compensates for this (in terms of required readout time) by being subdivided into quadrants that are read out in parallel. The placement of the bond pads (along the short edges of the device) was selected to permit a full-coverage multi-CCD geometry, and the dead regions along the long edges were minimized for the same reason. In short, the availability of affordable fully customized designs has transformed the possibilities for developing detectors truly tuned for particular requirements.

As well as the general layout, the devices can also be customized as regards the gate architecture. Generally three-phase clocking (as in Fig. 5) is preferred for the imaging area, but two-phase operation, with symmetrical clock pulses to minimize feedthrough to the analog-output, is advantageous for the R register. The noise performance and off-chip drive capability of the output circuit can be designed with the possibilities outlined in Sec. II D. This device was designed with four output ports, but a feature developed for other applications that will certainly be valuable in future CCD tracking detectors is that of multiport readout registers (with no loss of active area). The experimenter can thus balance the desired readout time against the volume of front-end electronics, which scales with the number of channels.

One vital topic will need to be addressed as clocking speeds are further increased. Despite the comments in Sec. II D, it has so far proved impossible to come close to a 50 MHz readout rate with $<100 e^-$ rms noise. The reason has been a serious level of interference (crosstalk) between the R

drive pulses and the sensing of the output voltage. The problem is partly on-chip but much more importantly in the front-end electronics. Sensing mV-level signals in the presence of ~ 10 V fast clock pulses has proved extremely difficult. The way forward probably relies on some developments in CCD architecture and changes in the front-end electronics. A promising approach appears to be to generate the R pulses locally to the register of the CCD, taking care with wire bonds and the trace layout on the CCD itself. It may even be possible to operate with balanced (opposite-phase) sinusoidal clock signals to minimize higher harmonics. This will involve some special features to inhibit R register transfer during the I-to-R shifting between rows.

In general, an increasingly intimate link between the CCD design and the front-end electronics design promises to open up important new horizons in the overall capability of these detectors in the near future.

F. Tracking performance

By the late 1970s, CCD development was at the point where their quality (uniformity, noise performance, etc.) made them valuable tools for astronomy. Particle signals had been observed in a related device (photodiode arrays),⁶⁰ although limited to the enormous charge disposition from 5.5 MeV α particles; the noise performance would not have permitted MIP detection.

The first observations of MIP detection in CCDs came from astronomers^{61,62} who saw cosmic ray signals as a background present particularly when they operated their instruments in telescopes at high altitude (thus ruling out background radioactivity as the source of these signals). Following a theoretical evaluation,⁹ the first measurement of efficiency ($>98\%$) and precision ($\sim 5 \mu\text{m}$) for MIP detection was made in a CERN test beam.¹⁰ Figure 12 from Ref. 10 opened the eyes of the HEP community to the potential for physics. With 17 hits over 1 mm^2 and no problem of cluster merging, it was clear that such devices could provide the basis for powerful vertex detectors. This development encouraged a number of other pioneering experimental studies with a variety of CCD architectures,⁶³⁻⁶⁷ all using off-the-shelf optical imaging devices available at the time.

The features of narrow band-gap and planar processing have already been mentioned as advantages of silicon CCDs for MIP tracking. There are in addition:

- (1) use of a relatively low-Z material;
- (2) intrinsically single-sided processing (unlike some tracking detectors), hence they can be thinned by mechanical lapping;
- (3) adequate signals from only $20 \mu\text{m}$ of material.

These features represent particularly important advantages for vertex detectors, in which multiple scattering in the detector layers is frequently a limiting factor in the topological event reconstruction.

In order not to be swamped by dark current, particle-tracking CCDs are generally cooled. Depending on readout conditions, quite modest cooling from room temperature (e.g., to 0°C) might be adequate in some applications, but as

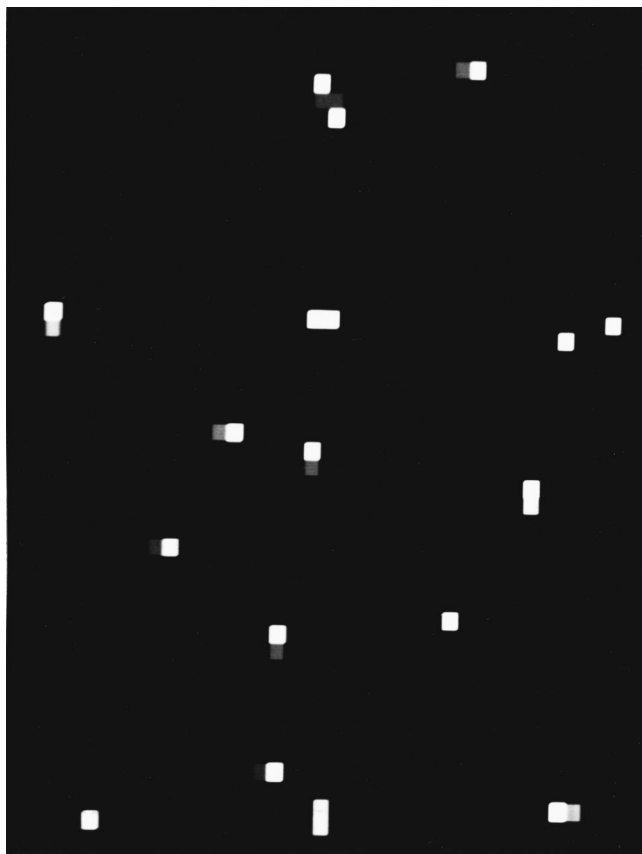


FIG. 12. One mm² of a CCD in a MIP test beam with every pixel of 20 μm^2 being read out. No threshold: Gray scale indicates the signal amplitude in each pixel.

will be discussed in Sec. V, radiation effects can be greatly suppressed by much more substantial cooling (and tracking CCDs are always operated in a radiation environment). All CCD tracking detectors so far used have been operated in the temperature range 150–200 K, which of course has implications for the mechanical and other design details, as mentioned in Secs. III and IV. Despite some early misgivings, this has not caused significant problems; it has in all cases been possible to engineer simple cryostats of extremely low mass which have been entirely adequate for the experimental requirements.

Early MIP signals, while generally confirming the more optimistic theoretical estimates of charge deposition referred to in Sec. II A, suffered from tails on the low side of the distribution which were identified with process defects in the devices available at the time. The improvements in processing quality since then have been impressive. Figure 13 shows the MIP signals from a large CCD (of the layout shown in Fig. 11) being read out at 5 MHz, where the scale is $\sim 30 e^-$, analog-to-digital converter (ADC) count. The electronic noise in this detector was $\sim 60 e^-$ rms, or 2 ADC counts. The now-standard signal processing procedure consists of effectively a two-pass approach. The locally digitized signals are transmitted in real time (by multiplexed optic fibers operating at 1 Gbit/s) to a rack of signal processing electronics adjacent to the overall detector. In the first pass (also carried out in real time during readout) addresses of pixels which satisfy a low threshold are provisionally stored,

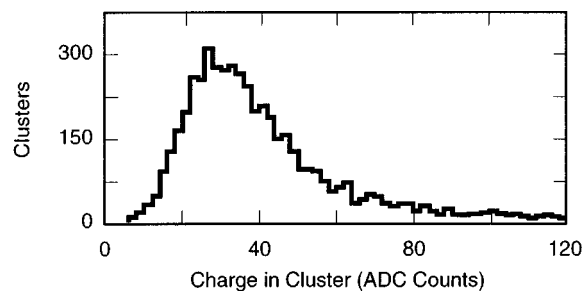


FIG. 13. MIP cluster signals from a large area CCD (data from the SLD).

along with the pixel signals from a generous surrounding region of interest (8×6 pixels total for every trigger pixel). The aim is to efficiently find clusters even in cases where the signals are split uniformly over a 3×3 area, as sometimes happens. Microprocessors look at the data from all these numerous “regions of interest,” assemble clusters using the data from pixels neighboring the one which triggered the first pass filter, and accept the cluster if a more robust cluster threshold of $\sim 250 e^-$ is satisfied. Figure 13 shows the cluster signal distribution for MIPs from such a detector. The entries in Fig. 13 are guaranteed MIP signals by the fact that the clusters have been subjected to a further offline filter; they are located on fitted tracks from a three-layer detector. In this way the prevalent backgrounds in the experimental conditions (due to x-rays, etc.) are excluded from the plot. This two-pass approach with final adjudication by a cluster threshold permits essentially 100% MIP detection efficiency to be achieved with very high noise immunity, as is essential in systems consisting of several hundred Mpixels if problems of data storage are to be avoided. In the absence of signals from ionizing particles, this signal processing leads to < 50 accepted noise clusters per CCD, of 3 Mpixels, a totally negligible level, and some of these accepted clusters are surely “real” (due to background radioactivity, etc.). Details of this signal processing procedure are described in Ref. 56, and references therein.

III. FIXED TARGET EXPERIMENTS

A. Detector design

As discussed in Sec. I, the purpose of the CCD tracker (vertex detector) within an experiment is to resolve tracks from secondary and tertiary vertices from those coming from the primary interaction vertex. As noted in Sec. II F, current CCD tracking detectors give a point measurement precision of $\sim 5 \mu\text{m}$ (by taking a simple centroid of the digitized data from a cluster of $20 \times 20 \mu\text{m}^2$ pixels). Of course, what is relevant for physics is not the precision at the detector plane, but that achieved after extrapolation to the interaction region (IR) close to the primary vertex (PV). By arranging CCD detector planes approximately at distances d and $2d$ from the PV, the typical precision at the IR will be $\sim 7 \mu\text{m}$. For low momentum tracks, multiple scattering in the first detector plane will degrade the precision, whereas for high momentum tracks the precision may be better than this, since information from more remote detectors can further refine the extrapolation. At first glance, an impact parameter precision

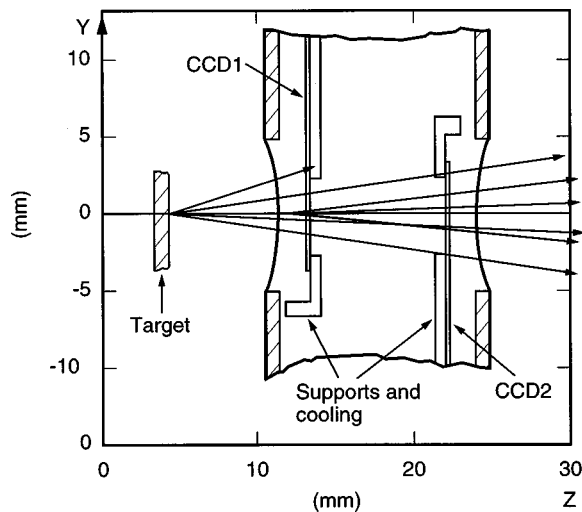


FIG. 14. CCD vertex detector for a fixed target experiment (NA32). Data are fast shifted into the quiet regions above and below the spectrometer aperture for CCDs 1 and 2, respectively, prior to readout.

of $\leq 10 \mu\text{m}$ appears to be more than adequate. Other than for low momentum parent particles with Lorentz boost $\beta\gamma \lesssim 1$, the mean value of the impact parameter of a decay track (the amount by which the extrapolated track misses the IP) is approximately $0.7c\tau$; $220 \mu\text{m}$ for B decays and $100 \mu\text{m}$ for charm. However, the desirable precision is far below these values, since some tracks will by chance pass close to two possible vertices, all distributions have significant tails, etc. In fact the experience to date (and this applies equally to the collider experiments discussed in Sec. IV) is that the physics reach is substantially increased as the vertex detector quality evolves; even today one falls short of anything like overkill in this aspect of the experiment.

Due to one particular advantage, high energy fixed target experiments provided the first environment in which silicon vertex detectors (both microstrip detectors and CCDs) were able to make a contribution to heavy flavor physics. This is the simple fact that in the Lorentz transformation from the center-of-mass (c.m.) to the lab system, the majority of the solid angle is compressed into a relatively small forward cone. Thus general purpose multiparticle spectrometers are typically long detector systems (tens of meters) with modest ($\sim 2 \text{ m}$) transverse dimensions. By using a well focused beam on a thin solid target, and by placing the silicon tracking detectors close to the target, very modest area coverage was required. Thus, the two-CCD vertex detector used in ACCMOR experiment NA32⁶⁸ covered the entire spectrometer aperture with only 0.4 cm^2 of CCD area even in the downstream detector plane (see Fig. 14).

As well as concentrating the relevant solid angle in a limited forward cone, the Lorentz boost provides a further bonus, plenty of space to the side of each active detector plane for frames, readout boards, cables, etc. With the massive local electronics required for the early detectors, this space was an essential requirement. Thus for the NA32 experiment, the only significant material generated by the CCD detector in the aperture of the experiment were the two layers of silicon. Even without thinning the silicon below the origi-

nal wafer thickness ($350 \mu\text{m}$) this implied a negligible multiple scattering penalty, again thanks to the effect of the Lorentz boost on the momenta of the decay particles.

The final advantage of the fixed target environment is the easy access to the detectors. In these conditions, radiation damage is not a major problem. The entire CCD detector system could easily be replaced once or twice a year; this was the practice followed in the NA32 experiment. In view of their favorable characteristics, the only reason why CCDs have not been more widely used in fixed target experiments (particularly for charm photoproduction, where the conditions would be extremely clean) seems to have been the relative unfamiliarity of these devices for tracking applications.

CCD tracking is not only of interest for vertex detection. Their very high precision can be exploited in constructing a compact high resolution spectrometer, in cases where the angular and momentum range happen to be small, so that large area coverage is not required. An example is a very high resolution e^+e^- pair spectrometer currently being prepared as part of a SLAC experiment.⁶⁹

B. Readout architecture

In contrast to the physical advantages noted in Sec. III A, a disadvantage of the fixed target environment was that the central region of the CCD active area was traversed by the high intensity primary beam. Consequential radiation damage problems could be minimized by defocusing the beam in the horizontal dimension (a beam profile $H \times V$ of $8 \times 0.3 \text{ mm}^2$ was used in this experiment), but the hadronic damage resulting from this beam (typically 10^6 particles/spill and a spill rate of 0.083 Hz) necessitated exchanging the CCDs every six months or so. The nature of the radiation damage effects will be discussed in Sec. V. Another consequence of the beam traversal was the continual generation during the spill of a huge number of hits in the active area of the CCD. Given the nonavailability of a true fast clear or fast latch feature on a CCD, these hits threatened to obscure the wanted data. A procedure was therefore devised to minimize this problem; the CCDs were clocked throughout the beam spill in the so-called fast clear mode. This consisted of a sequence of I shifts at 1.4 MHz so that the image was continuously shifted into the R register and dumped. Since only the remote one-third of each CCD was needed to cover the spectrometer aperture, it was possible to use the additional height of the device as a parallel analog storage region. On receipt of a trigger, the fast shifting continued until the required image region was in a "parking area" adjacent to the R register. Figure 15 illustrates the idea; an event generates a pattern of hits in the readout area (marked \times); these stored data are shifted vertically upwards/downwards in CCD1/CCD2 into the parking areas. The CCD drive sequence would then be changed to normal read mode, until the event had been read, thereafter reverting to fast clear and releasing the deadtime. During the relatively slow readout, the rows traversing the beam position vertically would encounter very high occupancies, but such regions could never contain valid data due to the system deadtime. In fact to keep conditions in the parking areas even cleaner, a small kicker magnet was

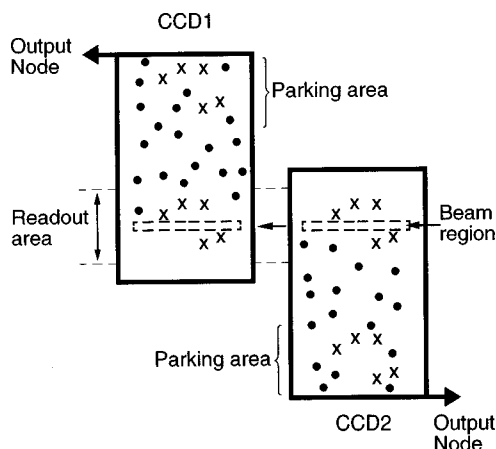


FIG. 15. CCD readout scheme for experiment NA32. Shown is a beam's eye view of the two CCDs of Fig. 14, with a relative sideways displacement between the CCDs for clarity.

used to dump the beam far upstream of the ACCMOR detector during readout, but this was barely necessary.

C. Physics performance

The NA32 experiment with the CCD/microstrip vertex detector provided some of the cleanest charm reconstructions of any detector system. Figure 16 shows one of the first charm decay events seen in the CCD-based vertex detector. The event-related hit density in the upstream detector (only 12 mm from the IP) was $\sim 200/\text{mm}^2$; no other class of tracking detector could come close to resolving hits at anything like this density. As can be seen, the beam-related hits in this experiment made a negligible additional contribution to this occupancy.

Given the harmonious conditions for CCD-based vertex detectors in the fixed target environment, the only reason to move out of this arena was the physics importance of processes at c.m. energies that could only be accessed at colliding beam facilities, and the need for heavy flavor identification in studying such processes. It was the overwhelming interest in such high energy processes that accounted for the requirement to develop vertex detectors able to face the major additional challenges of the colliding beam environment.

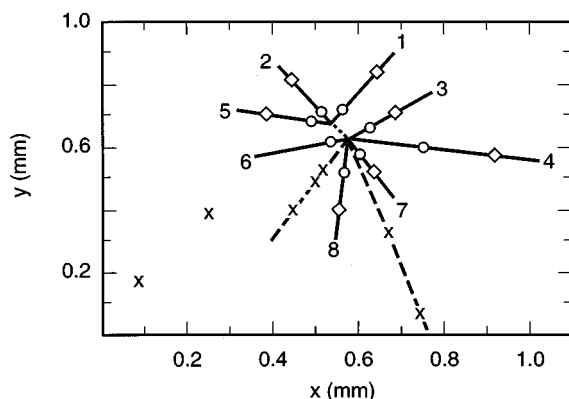


FIG. 16. Tracks from the IP and from a nearby charm decay in the NA32 vertex detector. The frame size is $1 \times 1 \text{ mm}^2$.

This was an onerous undertaking, involving (in the case of CCD detectors) around six years of intensive R&D work.

IV. COLLIDING BEAM EXPERIMENTS

A. Detector design

The main advantage of colliding beam experiments is the availability of c.m. collision energies far beyond the reach of fixed target experiments, and hence access to new physics processes. Against this overriding advantage, there are two main disadvantages. The first is the need for large solid angle coverage in all detectors, and the second is the fact that particle momenta are typically much lower than in the boosted fixed target environment and hence multiple scattering in tracking detectors is serious.

Regarding these problems, it seems at first glance that the ideal vertex detector would consist of a series of concentric thin spherical shells. But the fact that the beams are contained in a cylindrical pipe, and the advantages of placing the first detector layer as close as possible to the IP, lead inevitably to a cylindrical geometry for the innermost layer. From time to time there has been interest in using quasi-spherical shells further out (e.g., the 'lampshade' geometry) but optimized mechanical designs generally lead to a series of nested cylindrical barrels (made as thin as possible) with stable mechanical supports at the ends. For microstrip detector systems there may be an argument for short cylinders plus 'endcap' detectors (planes normal to the beam direction) since the track precision is degraded for oblique incidence. CCD detectors are essentially free of this problem, so in this case, 'long barrels' generally constitute the optimal design, unless one had some special reason for coverage at very small polar angles.

Both CCD vertex detectors constructed for the SLD experiment (called VXD2 and VXD3) have consisted of concentric barrels composed of 'ladders,' the basic building elements of these detectors. For VXD2 (for which work started in 1984) available CCDs (area $\sim 1 \text{ cm}^2$) limited the coverage severely. This detector is described in Ref. 70. Given the rapid progress with CCD developments, it became possible in 1994 to start design and construction for a new detector, VXD3, using much larger ($\sim 12 \text{ cm}^2$) full custom devices of the general architecture shown in Fig. 11. A full report on this detector has recently been published Ref. 56, so the details can be omitted here. Points of general interest are as follows.

First, the CCD design included features of importance for the mechanical construction. The on-chip circuitry was specially arranged so as to permit the sawn edge of the device to be within $300 \mu\text{m}$ of the edge of the active area, along the long edges of the CCD. The wire bonds were all located along the short edges, and displaced away from one edge to permit the ladders (Fig. 17) to be tiled in each barrel with small azimuthal overlap between adjacent active areas (Fig. 18). The active surface of each CCD was overlaid with evaporated aluminum squares of $60 \times 60 \mu\text{m}^2$ on a pitch of 3 mm, which were used as fiducials for purposes of optical alignment.

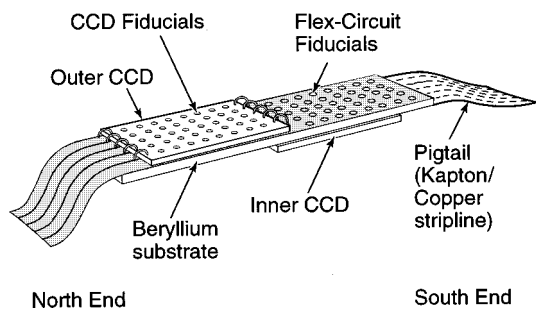


FIG. 17. Two CCD ladders that formed the basic elements of the SLD vertex detector VXD3.

The very thin, flexible ladders were mechanically stabilized by being firmly clamped at each end in the overall beryllium support structure (see Fig. 19). Due to the need to allow for controlled movements as a result of thermal cycling, the mechanical design incorporated a judicious arrangement of stress-relief features (sliding joints and elastomeric adhesives).

Since the total power dissipation in the cryostat due to the readout of the 307 Mpixels detector was only ~ 15 W, the detector could easily be maintained at its operating temperature (~ 180 K) by a gentle flow of cold nitrogen gas.

B. Readout architecture

Having established the desired general mechanical design for collider vertex detectors, let us consider the readout requirements. Unlike the fixed target applications, the full CCD area must be used as active detector; there is no scope for a "parking area" outside the active region. As the collider energy is increased, the need for high luminosity leads to high trigger rates. This is particularly true for "discovery" physics, where energy deposition in the calorimeter system may be small, and the energy threshold for a trigger is limited only by noise in the calorimeters. Therefore any detector needs to operate in a deadtimeless or short deadtime mode. In cases of high background rates, it is obviously desirable to incorporate a fast gating capability so as to latch the data associated with the triggering event. This requirement, easily met in most high energy physics detectors where the signal

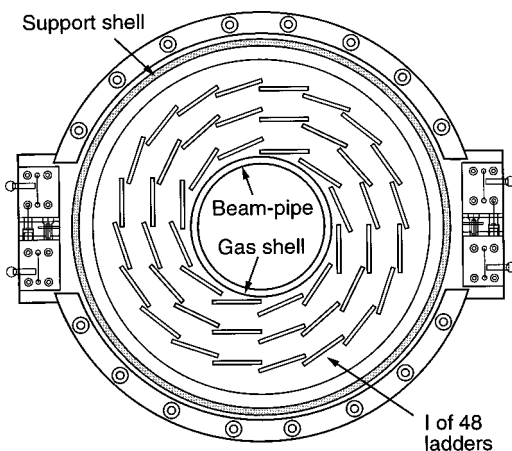


FIG. 18. Cross section (end view) of the VXD3 detector.

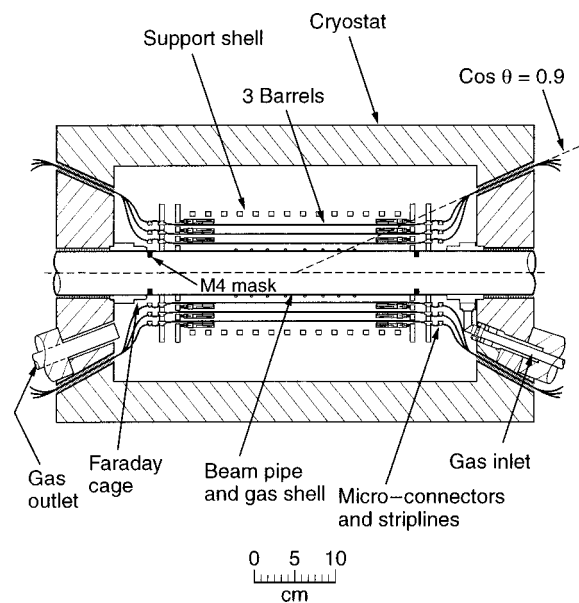


FIG. 19. Cross section (side view) of the VXD3 detector.

charge is collected promptly on external preamplifiers, is not an option available in a CCD detector. Thus all background during the readout is integrated with the signal. In principle, an equivalent of the kicker magnet used to kill the beam in fixed target experiments could be used. This is particularly simple if the background comes mainly from beam-beam interactions; one needs only to displace the beams out of collision during readout. This is of course ruled out in high trigger rate conditions by considerations of deadtime. The more widely used approach is to permit full-luminosity operation throughout the readout and, if a second trigger occurs, to simply continue reading until the corresponding full frame has again been acquired (deadtimeless operation).

In practice, CCD detectors are ruled out at hadron colliders for two reasons. First, instantaneous rates are excessive. Despite the large pp total cross section, and correspondingly the enormous rate of "minimum bias" events, these colliders have to run with very high luminosity in order to have a reasonable rate for the tiny fraction of interesting events. Second, CCD detectors would have inadequate life expectancy due to their sensitivity to hadronic radiation damage (see Sec. V). Note that this situation is quite different from the fixed target hadron beam experiments, where exchanging the CCDs every few months is neither too costly nor inconvenient. Nested barrels of detectors of ~ 1 m², buried inside thousands of tons of other delicate equipment, need to be far more robust.

In e^+e^- colliders, the hadronic backgrounds can usually be reduced to a very low level, so the radiation environment is generally tolerable. However, the instantaneous rates at high-luminosity machines such as the B factories now under construction would also rule out CCDs on grounds of occupancy. For the high energy e^+e^- colliders (LEP and SLC, at the present), the hit rates can easily be accommodated. The huge beam pipe at LEP was a major drawback, and indeed all vertex detectors there have been constructed with the simpler silicon microstrip technology. SLC, with its much

smaller beam pipe (2.5 cm, compared with 10 cm in LEP originally, subsequently reduced to 5 cm), provided a much more hospitable environment for vertex detectors, and with it a greater physics potential than LEP for a given luminosity. In fact, the SLC luminosity has been considerably lower than at LEP, and for this reason the heavy flavor physics results from the two machines have been of quite similar quality, up to the present time. What was really needed for physics was the LEP luminosity with the SLD vertex detector.

At SLC, the time structure of beam bunch crossings at 8 ms intervals lent itself to a convenient CCD detector readout architecture. Note that the front-end electronics could all be located outside the cryostat (Fig. 19) using thin copper-kapton flex circuits for the connections to the CCDs. Default operation consisted of fast clearing between beam crossings (analogous to the fast shifting used in the fixed target environment), so that the CCDs were relatively background free on receipt of a trigger, followed by standard readout during which the background of the succeeding 25 beam crossings was accumulated.

The generation of CCD drive pulses, the amplification of the analog signals, and the digitization of those signals all took place in the front-end electronics boards mounted within the aperture of the SLD central drift chamber, at small polar angle below the region of tracking. The digitized signals were multiplexed onto fast optical fibers and processed remotely, as discussed in Secs. II D and II F.

C. Physics performance

Key features of the VXD3 detector that placed it in a different category from the competition were

- (1) a small SLC beam pipe, hence small inner-barrel radius (28 mm);
- (2) thinned CCDs on beryllium substrates, giving thin ladders ($0.4\% X_0$);
- (3) a good lever arm from first to second layer, allowing precise extrapolation to the IR.

The performance of such a detector is best described by the impact parameter precision for tracks extrapolated to the IR as function of momentum. Results for this detector and for its predecessor VXD2 are plotted in Fig. 20, and can be parametrized approximately as

$$\sigma_{r\phi} = 14.0 \oplus \frac{33}{p \sin^{3/2} \theta} \mu\text{m},$$

$$\sigma_{rz} = 26.5 \oplus \frac{33}{p \sin^{3/2} \theta} \mu\text{m}.$$

In each projection, the impact parameter precision with VXD3 is at least a factor of 2 better than has been achieved with competing microstrip detectors at LEP. Given the low momentum of tracks in the e^+e^- collider environment, the multiple scattering term in the impact parameter formula is of the greatest importance.

Looking at the data from $Z^0 \rightarrow \text{hadron}$ decays in the SLD experiment, the impact parameter distribution is compared with Monte Carlo (Fig. 21). The remarkable agreement over

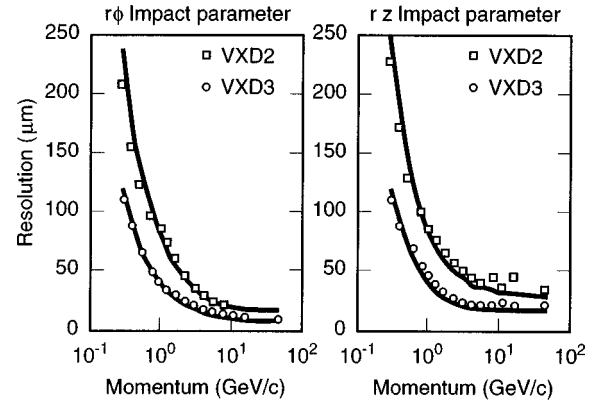


FIG. 20. Measured impact parameter resolution as a function of track momentum for tracks at $\cos \theta = 0$ for VXD2 and VXD3 compared with the Monte Carlo simulations.

four orders of magnitude demonstrates the degree of which the performance of this detector is understood and simulated.

The performance for a typical event is shown in Fig. 22. When the IR region is magnified, displaced vertices can be seen clearly; this was an event of type $Z^0 \rightarrow b\bar{b}$.

A great deal of heavy flavor physics has emerged from this experiment; see Ref. 71 for recent reports.

V. RADIATION DAMAGE IN CCD TRACKING DETECTORS

A. Introduction

CCD tracking detectors will inevitably be operated in a radiation environment, a situation also encountered by users of imaging CCDs in industry (nuclear, x-ray and electron microscopy, for example), for space-based optical and x-ray telescopes, etc. Radiation damage in these complex silicon devices is therefore relevant to numerous application areas and has been studied for many years. Reference 72 provides a particularly valuable review. Despite being 17 years old, it remains the most comprehensive general paper on this subject.

Despite these extensive studies, there is no simple picture that summarizes radiation effects of concern to all CCD

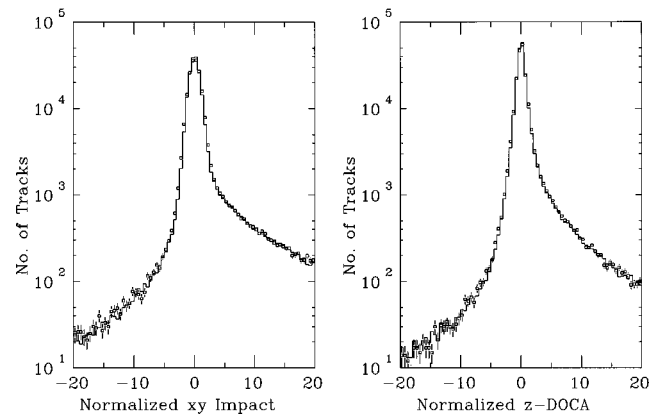


FIG. 21. Data (points) and Monte Carlo (histogram) distributions of the impact parameter with respect to the IP in $Z^0 \rightarrow \text{hadron}$ decays (VXD3 detector in the SLD experiment). The tails on the positive side are due to heavy flavor decays.

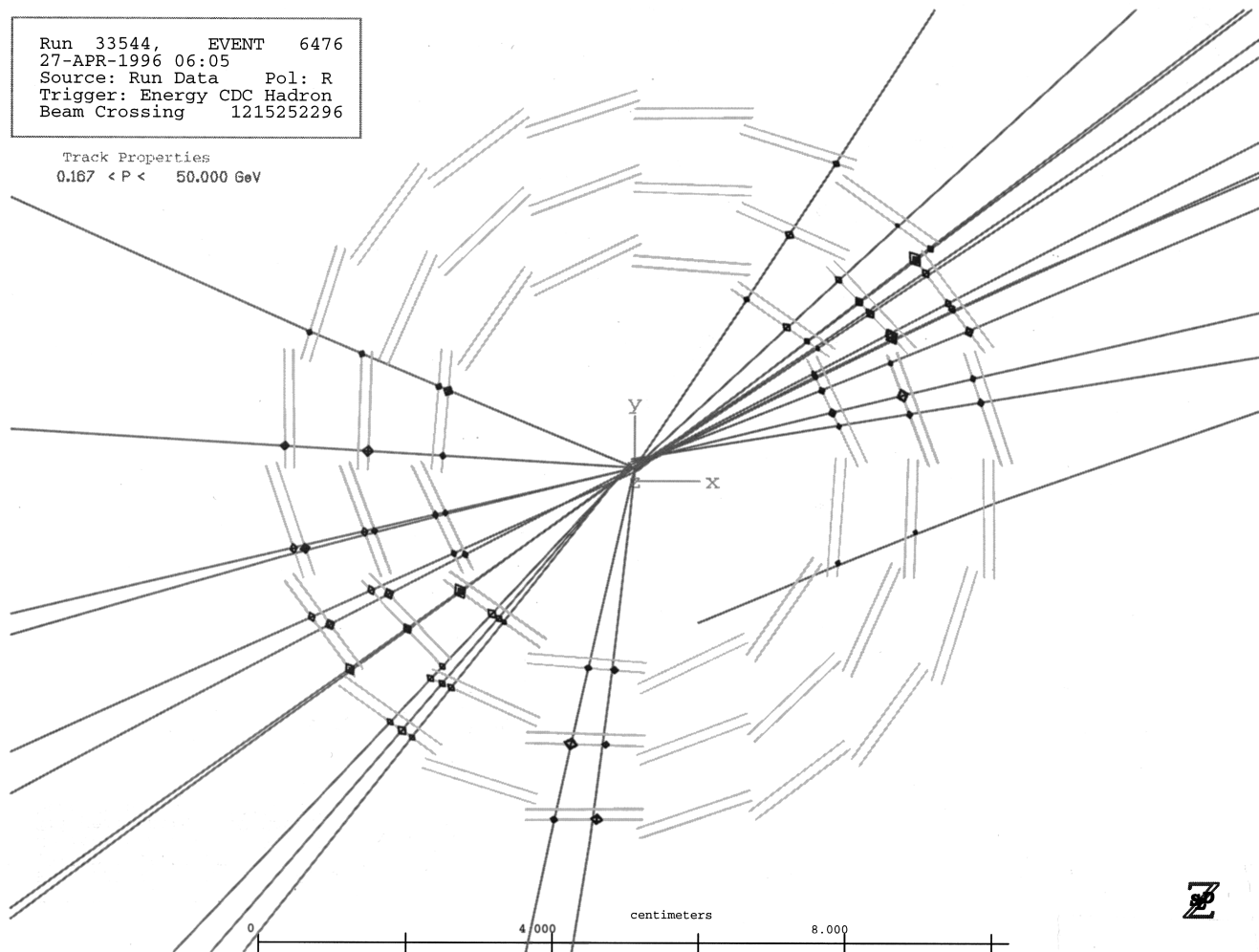


FIG. 22. End view of a detector with a reconstructed event of type $Z^0 \rightarrow b\bar{b}$.

users for two reasons. First, the uses made of these devices are highly variable. To a particle physicist (who is interested in the tracking precision given by the centroid of a MIP cluster) a 10% loss of signal (as long as it be slowly varying across the detector area) would not be serious. To an x-ray astronomer, using the cluster signal amplitude to determine the x-ray energy, such a degradation would be disastrous. Second, the radiation sensitivity depends strongly on the operating conditions, such as integration time, readout speed, etc. These conditions may be imposed by external factors peculiar to a specific application. For example, the limitations on operating temperature and power dissipation of space-based systems are likely to be more restrictive than in terrestrial applications.

In this section, an attempt is made to focus on the issues relevant to the particle tracking/vertex detector application, leaving aside issues of great importance to other users.

B. Surface damage

Let us consider the typical case of an n -channel CCD with dielectric consisting of equal thicknesses of SiO_2 and Si_3N_4 . The oxide layer has a band gap of 9 eV, and a mean energy for electron-hole generation of 18 eV. The electrons

and holes generated by ionizing radiation will (for a biased CCD) drift in opposite directions. The electrons have high mobility and are rapidly drifted into the bulk silicon. (Note that the drift direction would be opposite to this in the case of a p -channel device.) The holes (at temperatures ≥ 150 K) have sufficient mobility to drift within minutes to the oxide/nitride interface, where they have a significant probability of being trapped. For devices operated at much lower temperatures (e.g., liquid nitrogen temperature) the holes may remain essentially static within the oxide, but occasionally warming the detector would permit them to drift to the oxide/nitride interface or (if not trapped there) to be neutralized at the CCD gate electrodes.

In addition to fixed positive charge buildup within the dielectric, ionizing radiation causes an increase in the surface states (interface states) at the oxide/silicon interface. These interface states are primarily acceptorlike in the upper half of the band gap, and donorlike in the lower half. In a depleted n -channel device, the Fermi level leaves the donors neutral and the acceptors below E_f negatively charged. So the interface charge partially neutralizes the dielectric charge, which is one reason why n -channel devices have higher radiation tolerance (for ionizing radiation) than do p -channel ones.

Numerous procedures have been devised over the years

for reducing the radiation-induced charge accumulation ("hard oxide" technology). For a typical modern n -channel CCD with oxide and nitride layer thickness each 80 nm, the radiation-induced shift in flat-band voltage ΔV_{FB} is ~ 100 mV/krad for devices irradiated under bias. Devices with reduced dielectric thickness (but still good yield and stable operation) are available with $\Delta V_{FB} \sim 10$ mV/krad, and another factor of 10 reduction has been achieved in experimental devices.

The effect of the flat-band voltage shift is to progressively raise the potential of the CCD buried channel. If this shift exceeds ~ 2 V (i.e., after a dose of 20 krad with standard devices), charge transfer to the output node (whose potential, set by V_{RD} , does not drift up) will become inefficient. V_{RD} can be raised to compensate, implying also an increase in V_{DD} to preserve the output circuit gain. This can continue until V_{DD} reaches the limit set by overall voltage breakdown. With the development of the pyrogenic CCD hard oxide process,⁷³ the practical limit for ionizing radiation is >1 Mrad, which is entirely adequate for all CCD vertex detector applications contemplated to date.

The flat-band voltage shifts are greatly reduced (typically by a factor of 10) if the CCD power is off during irradiation. In collider applications, where the main background is accumulated during machine tuning, this at first looks like an attractive option. However, as we shall see, bulk damage effects are much more dangerous and these occur regardless of whether the CCD is biased or not. The inner layers of a vertex detector (sitting just outside a virtually radiation-transparent beryllium beam pipe) are uniquely vulnerable; no external radiation monitor will provide a useful dose measurement. It is therefore prudent to keep the detector operating at all times during accelerator operation; it should be run in fast-clear mode outside of data taking periods, using the induced signal current to monitor the radiation, and have an interlock to shut off the accelerator if this exceeds a safe level. The increase in flat-band voltage shift is a small price to pay for the vital protection against unacceptable bulk damage.

As well as causing flat-band voltage shifts, the interface states produced by ionizing radiation act as sources of electron-hole generation, i.e., increased dark current. In HEP applications, there is no reason not to design the tracking detector for operation at cryogenic temperature, thereby reducing the dark current to completely negligible levels.

Reference 74 provided the first insight into radiation-induced surface damage in CCDs. Other papers which describe the important early progress in dielectric hardening techniques are Refs. 75–81. Reference 82 provides a valuable review and report on recent developments.

C. Bulk damage

The term bulk damage refers to permanent radiation-induced changes to the crystalline structure of the bulk silicon. Most relevant for CCD particle detection are the changes to the n -type channel within which the electron signal charge is stored and transported. Bulk damage can be caused by electromagnetic radiation, for electrons above a

threshold energy of ~ 200 keV, determined by the minimum energy transfer of ~ 20 eV required to displace a silicon atom from the crystal lattice. Electromagnetic radiation always results in "point defects," simple complexes of vacancies (V) and interstitial atoms (I). The interstitials are benign and immobile, but the vacancies diffuse through the crystal until they form a complex with some atomic inclusions. In the phosphorus-doped n layer, they nearly always form a Si- E center, an acceptorlike P- V complex which lies ~ 0.45 eV below the conduction band edge.

Bulk traps can adversely affect the dark current, charge collection efficiency, and charge transfer efficiency. Even in heavily irradiated CCDs, the excess dark current can normally be dealt with by modest cooling. Given the thin epitaxial layer (~ 20 μm) from which the MIP signal is collected, the requirements made on minority carrier lifetime are not severe, and there is essentially no problem with charge collection into the potential wells. However, once the electron charge packet starts its long journey to the output node (possibly several centimeters, ~ 2000 pixels), the situation is far more dangerous. At every location where the charge packet is momentarily stored (and there are three such locations for every pixel of a three-phase CCD) there is a finite probability that some of the signal charge may be trapped, leading to loss of charge transfer efficiency. In order not to seriously degrade the signal-to-noise performance, the average CTI of a tracking detector in a large instrument should typically not exceed $\sim 10^{-4}$.

For hadronic irradiation, the situation is more complex, so let us first consider the case of a CCD that has suffered bulk damage from electromagnetic radiation, and whose n -channel is randomly populated with a single type of bulk trap. These acceptorlike defects have a high probability of capturing signal electrons which come within their electrical sphere of influence. This situation is described by a restricted case of the general SRH theory of carrier capture and emission from traps, in which only capture and emission of electrons from/to the conduction band play a part. Hole capture and emission are irrelevant since we are concerned with traps in depleted material. This situation has been considered by various authors.^{43,47,50}

Let us first take a qualitative look at the situation. As the charge packet is transported from gate to gate (within a pixel or between neighboring pixels), vacant traps that lie within the storage volume of the charge packet will tend to capture electrons. If the traps are already filled (either fortuitously, due to the passage of an earlier signal packet, or deliberately for this purpose by the injection of an earlier "sacrificial" charge packet), they will permit the signal electrons to pass undisturbed. Also, if the signal packet is transported at a sufficiently high clock rate that the dwell time τ_g under any gate is small compared to the trapping time constant τ_c , the signal electrons will pass. Also, if the trap emission time constant τ_e is small compared with the clock pulse rise/fall time τ_r , the trapped electrons will be reemitted in time to rejoin their parent charge packet. Only if electrons are trapped and held long enough to be redeposited in the next or later potential well, does the process contribute to a loss of

CTE. This is evidently a multiparameter problem with some room for maneuver.

Let us now look at the process quantitatively.

Assuming all traps to be initially empty, the CTI is given by

$$\text{CTI} = \sum_{j=1}^{N_F} F_j \times \frac{N_{tr}}{N_s} \left[1 - \exp\left(-\frac{\tau_r}{\tau_e}\right) \right].$$

N_F is the number of phases per pixel (3 for a three-phase structure).

F_j is the fill factor for phase j , i.e., the probability that a trap in the charge packet storage volume will become filled during the dwell time.

$$F_j = 1 - \exp(-\tau_g/\tau_c).$$

For most cases of practical interest τ_c is ~ 10 ns and F_j may be taken to be unity. N_{tr} is the trap density and N_s , the signal charge density, is a function of the signal size. For very large charge packets, ($\geq 10^5 e^-$) it is approximately equal to the n -dopant concentration, but for signals N_e in the MIP range one finds $N_s \propto 1/N_e$ since the signal electrons occupy a constant volume determined by their thermal energy and the three-dimensional potential well in which they are stored. The CTE for small signals is correspondingly reduced.⁸²

Now

$$\tau_e = \frac{\exp[(E_c - E_{tr})/kT]}{\sigma_n X_n v_n N_c}.$$

The terms in the denominator are in turn the electron capture cross section for that trap type, an entropy factor, the electron thermal velocity, and the effective density of states in the conduction band. The numerator tells us that for shallow traps (or high temperature) τ_e is likely to be short and, conversely, for deep traps and/or low temperatures, τ_e is likely to be long. In fact, for deep traps and appropriate clock times, by reducing the temperature, one can sweep the CTI through its full range from approximately zero (since the charge is reemitted into the parent pixel during the drive pulse risetime) to $3N_{tr}/N_s$ (for a three-phase CCD) and back to zero, as all traps are filled by some long preceding deliberate or accidental charge packets to have been clocked out of the device. Figure 23 nicely illustrates this point. This demonstrates the growth in CTI due to irradiation of a CCD with a radioactive β source. The density of Si-E centers increases, but the effect on CTI can be minimized by operating at or below 190 K, where the trap emission time becomes adequately long. For this trap, the emission time constants at 210, 190, and 170 K are 69 ms, 1.06 s, and 31 s. The degradation in CTI below 160 K (even before irradiation) is not seen in later CCDs from the same manufacturer. It probably represents an artifact of the register design or processing of this particular device. In practice, one can normally reduce the operating temperature to ~ 85 K before the CTI rises to $\sim 10^{-4}$ at the onset of "carrier freeze out," the trapping of signal electrons by the phosphorus donor ions.⁵⁰ This effect sets an effective lower limit to the useful operating temperature of n -channel CCDs.

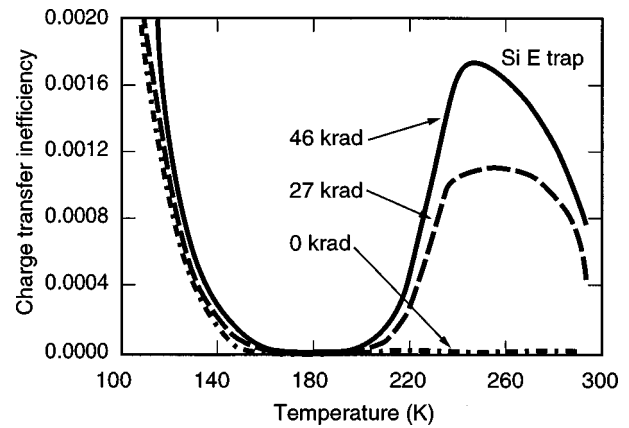


FIG. 23. Effect of ionizing radiation damage on CTI as function of operating temperature (^{90}Sr β source) (from Ref. 82).

For hadronic irradiation of CCDs, because of the much greater nonionizing energy loss (NIEL) factor,^{83,84} the damage rates are greatly increased, as is the complexity of the damage process. Charged hadrons such as protons have a large cross section for Coulomb–nuclear scattering with sufficient energy transfer to the struck silicon atom to not only displace it but to generate a cluster of further displacements. Neutrons have smaller interaction cross sections, but they induce nuclear disintegration which creates even larger damage clusters (having dimensions typically hundreds of angstroms in longitudinal and transverse dimensions). These clusters constitute highly disordered regions within the crystal, and may be a source of mobile vacancies, divacancies, etc. In the heavily doped CCD n channel, after hadronic irradiation the majority of active defects are again Si-E centers, but there are additional significant traps at $E_c - 0.4$ eV, believed to be the divacancy (VV),⁸⁵ and shallower traps at $E_c - 0.30$ and -0.12 eV.^{85,86} Protons are the most damaging; Fig. 24 shows the CTI resulting from an irradiation with the very modest dose of 3.6×10^9 10 MeV proton/cm². The effect of the lower level traps is to extend charge trapping into

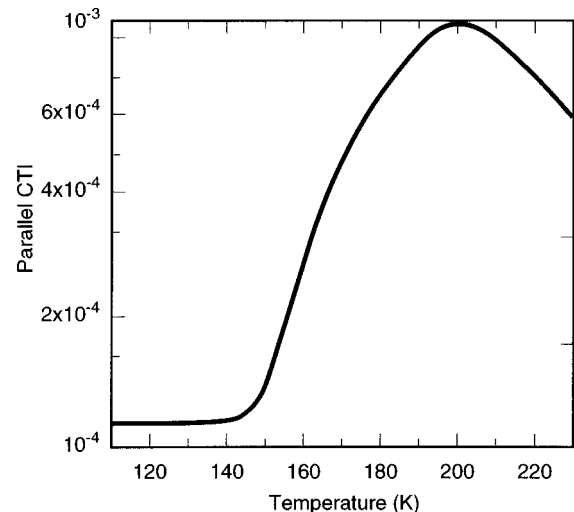


FIG. 24. Effect of hadronic radiation damage on CTI as function of operating temperature (10 MeV protons) (from Ref. 85).

the low temperature region, so the problem of degraded CTE no longer has a clear solution by cooling.

While these proton damage results are of great importance for their particular application area (space-based x-ray cameras), they probably give a pessimistic impression for the conditions relevant to particle detection systems for two main reasons. First, these results refer to very low signal densities, so the benefits of the long trap emission times at low temperature are not exploited to the extent possible in a particle physics experiment. Second, the only hadronic backgrounds likely to be significant at an e^+e^- collider are neutrons leaking through the shielding. There is evidence that neutrons may be much less harmful than would be inferred from these proton data. Taking the standard NIEL factor, the data of Fig. 24 correspond to an equivalent dose of 1 MeV neutrons of $3 \times 10^{10} \text{ n/cm}^2$. Yet there are measurements on n -channel CCDs (buried channel), which demonstrate CTI $\sim 10^{-4}$ for $3 \times 10^{12} \text{ n/cm}^2$ at a temperature of 140 K.⁸⁷ In these measurements the time between charge packets was only 10 ms, but there is evidence that at this temperature there was little CTE degradation by increasing this time to 10 s. There is the further difference that the neutron studies have all been made with large signal packets, but from Ref. 82 the degradation in CTE going from larger signals down to packets of $\sim 1000 \text{ e}^-$ was only a factor of 2 in material irradiated to 60 krad (beta source). Therefore the sparse measurements of the effect of hadronic damage on CTE in CCDs are not internally consistent to better than a factor of 100. It is possible that the simple application of the NIEL for proton/neutron comparison is not valid. A low density of massive damage clusters may be less harmful (for CTE) than a high density of small damage clusters. Improved experimental data are urgently needed.

D. Discussion

Due to their long readout time, CCDs are not applicable as vertex detectors in continuous high flux environments such as the LHC. They would also be completely ruled out in such an environment due to the high hadronic background. CCDs have a proven record in fixed target experiments (where the incident beam can be interrupted during the readout) and in the e^+e^- linear collider environment, where the interval between bunches (or between bunch trains) allows time for readout. In both these environments, radiation damage effects have so far been modest. In the fixed target environment, given the small number of CCDs required, they can simply be exchanged at intervals of six months or so. For the e^+e^- collider, with reasonable care over beam conditions, the detector lifetime can be many years.

For the future e^+e^- linear collider, the backgrounds may be substantially higher. The dumps for secondary e^+e^- pairs, for beamsstrahlung, and for the residual main beam are all significant sources of neutrons. At this stage, it is not clear if any of these could cause problems for a CCD vertex detector. As we have seen, there is an apparent discrepancy between the radiation damage data with neutrons and with protons as regards charge transfer efficiency, so the actual performance limits for a CCD detector are far from clear.

What is long overdue is a comprehensive study of the

radiation effects in one CCD design, comparing electromagnetic, neutron, and charged hadron irradiation, with particular attention to the operating conditions (clocking, charge injection interval, and temperature), covering the region of interest for particle detection. It should be noted that very high clocking rates for the readout register ($\sim 50 \text{ MHz}$) are envisaged for this environment in the future. This will provide a significant suppression of CTI in this register due to the fact that τ_g will no longer be much larger than τ_c , so the fill factor discussed in Sec. V C can be far from unity. Equally important as these systematic studies of radiation effects is a serious evaluation of neutron background conditions likely to be encountered at the future e^+e^- linear collider (the next major application area for a large scale CCD vertex detector). This work will reveal if there are any problems with the continued use of currently available CCDs in this field. Should there be difficulties with the anticipated neutron fluxes, there may be considerable room for improvements in the CCD design, as will be discussed in Sec. VI.

VI. FUTURE PROSPECTS

A. Developments in silicon CCDs

Globally, the market for CCDs for scientific applications will continue to grow, and to underpin the development of larger, faster, thinner, more radiation-resistant devices. General developments in the silicon planar process for the mass market (e.g., to feature sizes of $0.1 \mu\text{m}$ and below) will filter through to CCD processing (first to mass market devices, and finally to the scientific market). Those interested in building CCD tracking detectors will of course profit from all these developments. Despite the small scale of this market it is likely that its role can continue to be much more than that of passive “users” due to various factors.

First and foremost, as physicists, these users have a natural interest in the operating principles of their detectors and are always thinking of novel architectures and operation modes, some of which have proved to be of general applicability. Second, working in a field that pushes the limits of analog and digital electronic processing, high energy physicists are well placed to advance the readout possibilities of these detectors. During the past 20 years, the most important contribution by CCD tracking detectors to other fields has been the speeding up of readout with $< 100 \text{ e}^-$ rms noise from 10 kHz to 10 MHz. Work is already underway to achieve another factor of 10 speed enhancement. Third, as physicists with an excellent knowledge of the effects of radiation on materials, this community is very active in efforts to improve the radiation hardness of a wide range of silicon detectors including CCDs.

This review article has concentrated on the device architecture that currently has provided the most successful particle tracking detectors. However, this picture will continue to evolve, and it may be useful to at least mention current R&D which could open up new opportunities for tracking detectors.

Regarding spatial precision, the current values of $\sim 4 \mu\text{m}$ are normally adequate, particularly since the IP im-

pact parameter precision is dominated by multiple scattering for most tracks. Should higher precision be required for some particular applications, there are good prospects of achieving it. Reductions in readout noise (discussed later in this section) and/or increased signal through greater active layer thickness are feasible. It has long ago been established that, as regards sensitivity, the pixel-to-pixel uniformity of CCDs is generally so good that submicron ($\sim 0.1 \mu\text{m}$) precision in centroid finding is achievable. Submicron precision has been demonstrated both with defocused star images for satellite guidance systems⁸⁸ and with x rays,⁸⁹ and could undoubtedly be developed for MIP tracking if required.

Regarding radiation hardness, the performance for ionizing radiation is generally more than adequate, but the bulk damage picture for neutron irradiation is somewhat confused. This needs to be carefully studied with standard modern devices, plus variants that have been developed for increased hardness to proton irradiation. The most promising variants are those which reduce the signal charge storage volume, by higher levels of *n*-channel doping and/or narrow or supplementary channels.^{90,91} Such variants have reduced charge storage capacity compared with standard devices, but MIP signals are a factor of 100 below these levels (typically $10^5 e^-$), so this is certainly not an issue. More speculatively, one can consider whether *p*-channel devices would have improved hardness with respect to neutron bulk damage. They have been shown to have good resistance to ionizing radiation,⁸⁰ and their hardness to hadronic irradiation will soon be measured, given the expanding markets for radiation-resistant CCDs.

As well as *n*- and *p*-buried-channel CCDs (plus the surface-channel options which are probably not of use as tracking detectors), the junction or *pn* CCD offers another interesting category of devices.^{92,93} For applications such as x-ray detection, they have some advantages and some disadvantages (see Refs. 38 and 94 for recent reviews of each), and it may well be that there is a niche for these devices in some tracking detector applications.

Finally (and most important) on the shopping list of desirable CCD upgrades is the question of improved responsiveness of the output circuit, and hence improved signal-to-noise (S/N). This interest is driven not so much by the requirement of more precise signal measurement at current clocking frequencies, but by the need to achieve similar performance at much higher speeds. There is an ongoing impressive program of node capacitance reduction within the present floating diffusion plus source-follower output architecture, with a limit of $\sim 10 \text{ nF}$ being achievable.³³ Figure 25 illustrates the improvement in high speed noise performance with some recent realizations of this architecture. Beyond this, the "floating surface detector" of Brewer⁹⁵ has been refined and named the "double gate floating surface detector."⁹⁶ In this latter paper, spectacular responsivity ($220 \mu\text{V}/e^-$) and noise performance ($0.5 e^-$) are reported at a pixel clocking frequency of 3.6 MHz. In this beautiful architecture, the signal charge is stored beneath a *p*-type conducting channel of a surface-channel (enhancement mode) output FET. There are some design issues regarding implementing such a structure on CCDs with the relatively thick active layers convention-

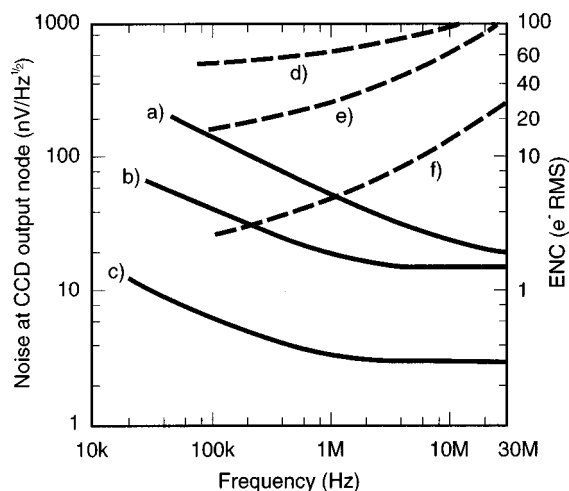


FIG. 25. Noise spectra (LH axis) of (a) surface-channel and (b) buried-channel devices as used in the SLD experiment. (c) The performance of a currently available state-of-the-art design. (d)–(f) The corresponding CDS noise performance (RH axis).

ally used for particle tracking purposes, but with such noise performance, one could reduce the thickness considerably and still expect adequate S/N at high clocking frequency.

It should also be noted that the possibility has recently emerged of incorporating a fast-clear capability in frame transfer CCDs, without loss of MIP efficiency. The idea is to build gated antiblooming drains, allowing clearing times below $1 \mu\text{s}$, in devices with reasonably thick ($20\text{--}30 \mu\text{m}$) epitaxial layers. A MIP traversing the drain region would lose a small fraction of the signal (that in the depletion region) but (by reference to Fig. 4) could still be detected with 100% efficiency by virtue of the signal collected by diffusion from the undepleted epitaxial material. This option would only be really useful in conditions where the background could be switched off (e.g., by a kicker magnet) during readout.

B. CCDs in new materials

Despite their many advantages for particle tracking, it is clear that silicon CCDs have certain limitations (speed, radiation-hardness) which rule them out in some areas. In some cases (see Sec. VI C) conditions may dictate radical non-CCD solutions, but there may be situations in which currently available CCDs are ruled out, but in which much higher speed, more radiation-resistant CCDs would be applicable.

In these cases, GaAs CCDs with GHz rate capability and excellent radiation hardness can be considered. The ongoing progress with band-structure engineering⁹⁷ could in principle lead to some very favorable device characteristics. After some remarkable early progress, reviewed in Ref. 98, these developments seem to have lost momentum. Even if imaging devices with the required performance become available, the application to particle tracking will not come easily. The requirements of large area coverage, minimal thickness (in radiation lengths), and mechanical robustness all raise significant barriers to the use of this material.

C. Active pixel sensors

In particle tracking applications where silicon CCDs are clearly ruled out (for example, at the LHC where beam-crossing rates and hadronic radiation levels would be prohibitive), the needs for pixel-based tracking detectors must be met by a radically different approach; the active pixel sensor (APS).

APS devices have for many years been suggested to displace CCDs as the preferred technology for optical imaging.⁹⁹ While it is clear that every technology has a finite life expectancy, the dominant technology at any given time is very difficult to displace. This situation was nowhere better illustrated than in the history of CCD imagers. Since their invention in 1970, they consistently failed to find a significant market in video cameras for 15 years; the vacuum tube devices were continually refined and remained ahead of CCDs throughout this period. While there are very exciting developments taking place with MOS APS devices, and already they are the technology of choice for certain low cost (and low image quality) applications, they have a long way to go to catch up with modern CCDs for high quality imaging purposes. This may well happen over the next decade, in which case APS particle tracking devices will be able to profit from that large market, as silicon CCDs currently do. But in the meantime, the particle tracking APS devices are being developed specifically for this very challenging application area.

The key characteristic of these devices which will permit them to function in areas where CCDs are prohibited is local charge sensing circuitry in every pixel. This naturally permits fast gating of the signals; and the freedom from transporting the signal charge through large distances in the semiconductor eliminates the overriding radiation softness of the CCD technology. There are two main classes of APS design, monolithic and hybrid. In the monolithic design (and this is the class pushed for imaging applications) the detector volume is integrated on the same IC with the readout electronics, while in the hybrid approach, a detector chip is bump bonded to a readout IC. The latter architecture is in some respects simpler to engineer, and all the pioneering APS detectors currently in use or envisaged for particle tracking are based on the hybrid technology. APS detectors fall outside the scope of this review, but should be mentioned briefly by way of explanation of the complementary application areas between these devices and CCDs as pixel-based tracking detectors, now and in the medium-term future.

Numerous monolithic APS structures have been shown to have capability for optical imaging, including the amplified MOS imager (AMI),¹⁰⁰ charge modulation device (CMD),¹⁰¹ bulk charge modulated device (BCMD),¹⁰² base stored image sensor (BASIS),¹⁰³ static induction transistor, (SIT)¹⁰⁴ and a variety of complementary MOS (CMOS) sensors, e.g., in Refs. 99 and 105. Typically, the unit cell of these devices consists of a photodetection volume coupled to a few transistors (for readout, selection, and reset). All these devices have the advantage with respect to CCDs that the signal charge does not need to be transported through the silicon, but the disadvantage that some or all of the carefully

crafted circuitry built once on the periphery of a CCD (with essentially no space constraints) now occupies real estate in every pixel and is repeated maybe a million times. To date CMOS imagers have established a role as relatively noisy devices in low cost imaging applications, where integration with signal processing circuitry is more important than image quality (e.g., in robotic control systems). However, since the minimum photolithographic feature size has decreased since the invention of the CCD from ~ 10 to $\sim 0.1 \mu\text{m}$, the possibility for greatly increased integration of logic within each pixel is rapidly advancing. It may well be that the boundary line between these classes of imager will move in favor of APS devices in the future, but this is not yet clear.

Much of the problem with APS devices relates to their inferior noise performance. One idea for dramatically improving this is by integrating an avalanche photodiode (APD) into a pixel imager. The drawback of APDs has been poor gain stability, but there are procedures for introducing negative feedback¹⁰⁶ which could solve this problem. There remain serious issues of crosstalk between neighboring cells due to light generation in the avalanche process; here again there are possible solutions.¹⁰⁷ This is an area with vast potential, but it could be a slow development process.

There have also been pioneering developments of monolithic APS devices for particle tracking/x-ray detection.¹⁰⁸ However, the APS systems currently used^{109,110} and those under development^{111,112} for particle tracking follow a rather different approach. Being hybrid devices, they consist of a simple array of *pin* diodes as the detector elements, using the same technology as silicon microstrip detectors. To this are bonded readout chips with relatively complex processing logic in each pixel, and consequently large area pixels (currently up to $10^5 \mu\text{m}^2$, aiming for $\sim 15\,000 \mu\text{m}^2$ in the future, compared with $400 \mu\text{m}^2$ for CCDs). These devices, designed for very high rate operation, use a column parallel architecture. A hit pixel sends its row address to a clocked shift register at the edge of the active area (one register per column), in which this information is shifted, to be latched and transmitted off-chip in the event of a level-1 trigger being received at a standard delay ($\sim 1 \mu\text{s}$) relative to the triggering event. Major challenges (compared with the optical APS devices) are presented by the small MIP signals and high rate operation (25 ns bunch crossing interval). As a result, present designs have relatively high power dissipation ($\sim 1 \text{ W/cm}^2$, approximately 100 times that of a CCD detector).

The combination of relatively large area pixels, much greater thickness, and high power dissipation (which necessitate additional material for cooling) makes APS devices relatively unattractive, compared to CCDs, as vertex detectors. They should and will be used in areas where the high crossing rate and/or radiation background completely exclude CCD vertex detectors, such as at the LHC. In the long-term future, it is certain that ongoing developments in IC technology (particularly in photolithographic feature size) will lead to major improvements in the performance of APS vertex detectors (hybrid or monolithic) even in these harsh experimental conditions.

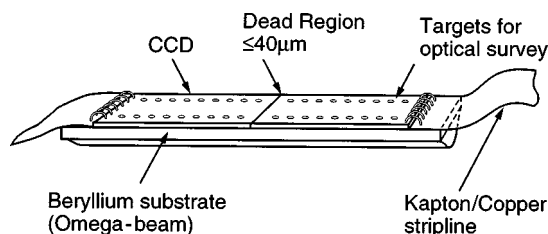


FIG. 26. Conceptual two CCD ladder design for a vertex detector at the future International Linear Collider. The beryllium omega-beam substrate is no thicker than that for VXD3, but it is over 50 times more rigid.

D. Discussion

The use of CCDs in fixed target experiments can be expected to continue in miscellaneous application areas where high precision, and/or high granularity are required over a modest area. Tricks such as the division of the device into an active area and a parking area will continue to allow clean operation in apparently hostile conditions. However, with the high energy frontier having passed irrevocably into the arena of colliding beam machines, the scope for new fixed target experiments is likely to continue to diminish, and with it support for advanced detector developments.

In the collider environment, APS devices will provide the only possible route to pixel-based vertex detectors in the hostile environment of hadron colliders, but the high energy e^+e^- linear colliders will continue to provide a natural niche for CCD-based detectors. Both for precision Standard Model physics and for discovery physics at such a machine, high quality vertex detection will be essential, and probably the

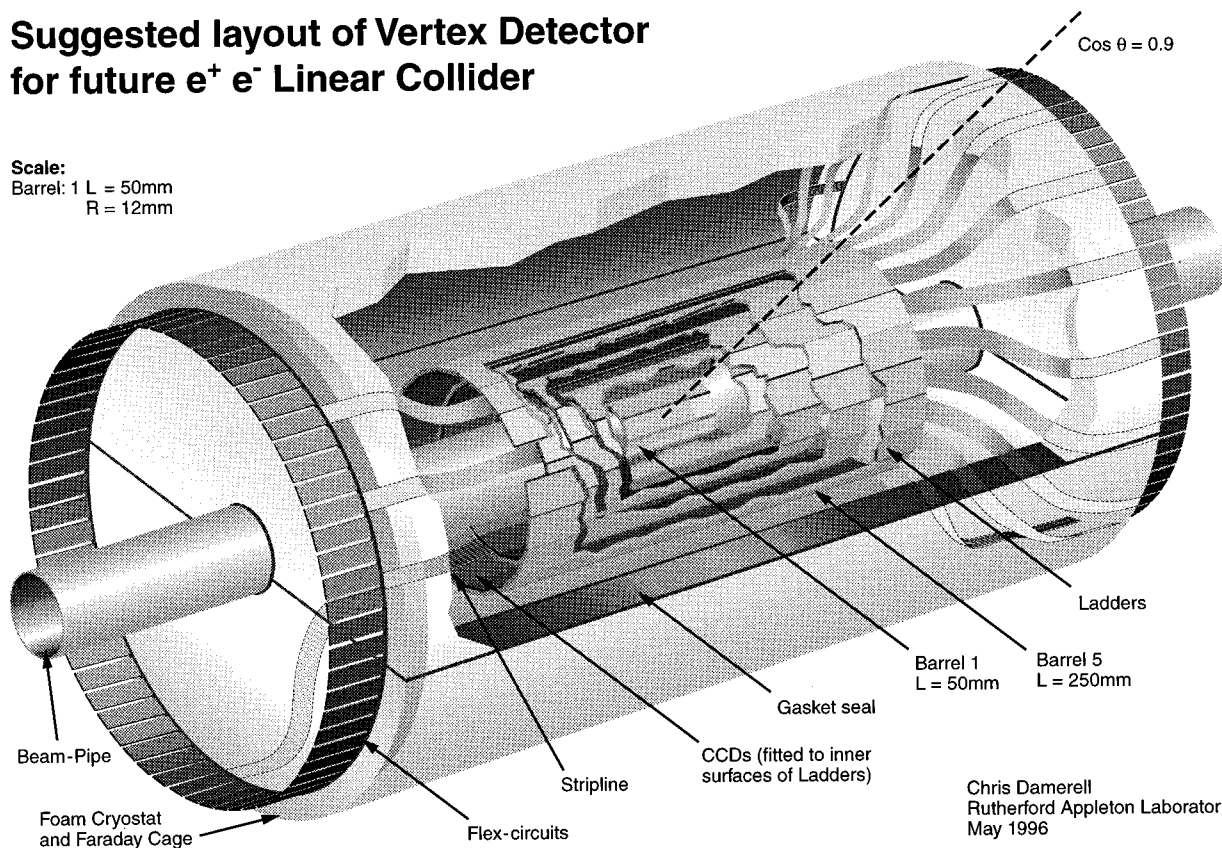
key to the discovery of new heavy particles (SUSY or otherwise) just as vertex detectors at the CDF played a vital role in the discovery of the top quark.¹¹³ For the future Linear Collider (which could be running on a timescale of around 2005) an ambitious R&D program is expected to lead to a CCD-based vertex detector with spectacular physics capability.¹¹⁴ The key to achieving this physics potential is to get really close with the inner layer (radius ~ 10 mm) and to reduce (to $\sim 0.12\%$ X_0) the layer thickness even below that achieved at the SLD. The conceptual ladder design is shown in Fig. 26, and an isometric view of the overall detector in Fig. 27.

The first of these aims depends on ongoing close cooperation between the accelerator designers and the detector physicists. At the present time, fully detailed studies of the flux of background radiation at this machine¹¹⁵ support the possibility of achieving this ambitious goal for the vertex detector radius; the physics payoff is impressive. The reduced layer thickness relies on CCD developments that have mostly been made in recent years for other application areas; see Ref. 114 for a full discussion.

The major background seen by this detector will be e^+e^- pairs produced by the beam-beam interaction. Even at the smallest radius, the radiation damage effects from this background are modest. Therefore as regards radiation damage this machine will be quite benign, provided that the various sources of neutron background (which emanate from the radiation dump areas) can be controlled. The main challenge in moving so close to the IP is sorting out the background hit

Suggested layout of Vertex Detector for future e^+e^- Linear Collider

Scale:
Barrel: 1 L = 50mm
R = 12mm



Chris Damerell
Rutherford Appleton Laboratory
May 1996

FIG. 27. Cutaway isometric drawing of the suggested five-barrel vertex detector. All associated electronics are external to the cryostat, in the small-angle region below the limit of tracking.

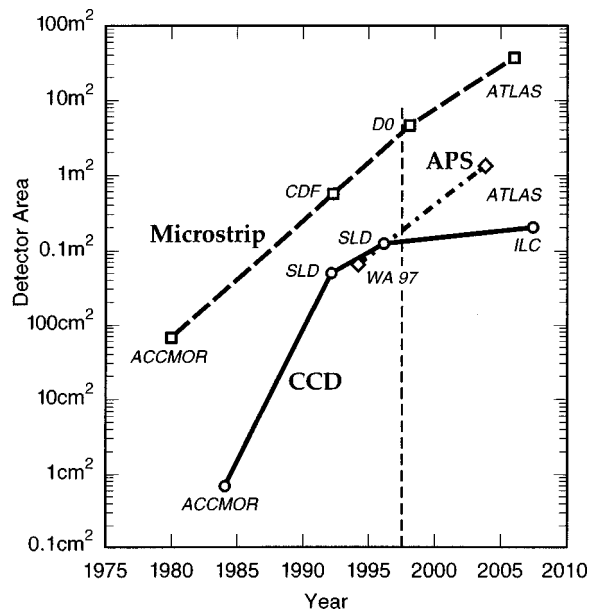


FIG. 28. Active area of the silicon vertex/tracking detectors as function of time. Microstrip detectors retain the capability of largest area coverage.

rate in the event reconstruction. This will be minimized by running the readout electronics faster by a factor of 5 than has been achieved to date (pixel clocking rate of 50 MHz). As discussed in Sec. VIA, there are several options for achieving this goal, although it will involve a significant R&D effort over the next few years. The most promising approach is probably to generate the balanced two-phase R drive pulses locally to the CCD, possibly with a sinusoidal wave form to minimize higher harmonics, and to use a high-sensitivity (three-stage) output circuit. There are ideas (still to be proven) for achieving the I-to-R transfer while preserving the sinusoidal R clocking.

Figure 28 illustrates the area coverage of various leading-edge tracking detectors in the silicon microstrip, CCD, and APS technologies as a function of time. Microstrip detectors remain in the lead, with APS detectors set to overtake CCDs on the LHC timescale. Seen in terms of numbers of channels (Fig. 29) the picture is different. CCDs are far in the lead and are likely to remain so in the foreseeable future. As regards vertex detectors, one valid rule is "small is beautiful," at least as regards the inner layer radius. This is illustrated in Fig. 30, which shows that ongoing pressure on the layer thickness and beam-pipe radius have paid off in physics reach in the e^+e^- linear collider environment, and this trend is set to continue in the next generation of these machines.

In short, CCD tracking detectors with $\sim 10^9$ pixels and $\sim 0.1\%$ X_0 /layer will provide state-of-the-art heavy flavor identification well into the next millennium. Only in environments where backgrounds are excessive will they need to be displaced by less precise alternative technologies.

ACKNOWLEDGMENTS

In this review article, an attempt has been made to summarize a large body of work undertaken by physicists and engineers from a variety of disciplines within the academic community and the semiconductor industry. As regards my

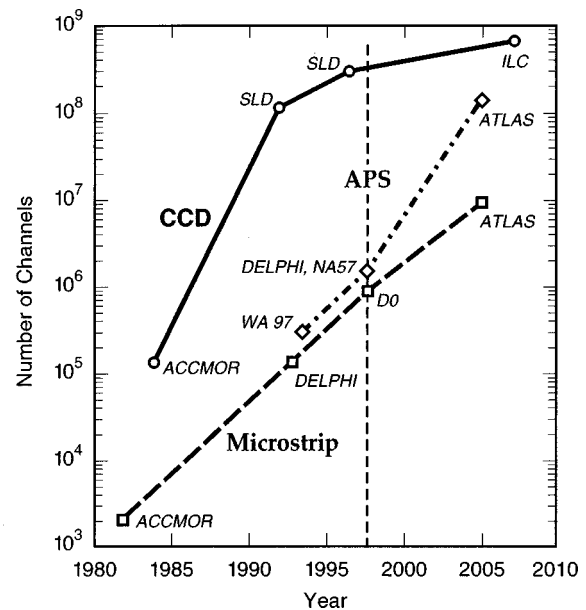


FIG. 29. Number of channels in the silicon vertex/tracking detectors as function of time. CCD-based pixel detectors retain the capability of finest granularity, but APS detectors may come close in the long-term future.

own work with CCD-based detectors, this has been carried out over the past 20 years with many colleagues drawn largely from the ACCMOR collaboration (CERN), the SLD collaboration (SLAC), and the CCD group led by David Burt at the General Electric Company (GEC) (UK). Too numerous to mention by name, their comradeship and brilliant ideas have made this work an adventure and a source of deep satisfaction. I thank them sincerely, hope they have all enjoyed it as much as I have, and can assure them that the best has yet to come!

NOMENCLATURE

ACCMOR: Collaboration working at CERN in the '70s and '80s
AMI: amplified MOS imager
APD: avalanche photodiode

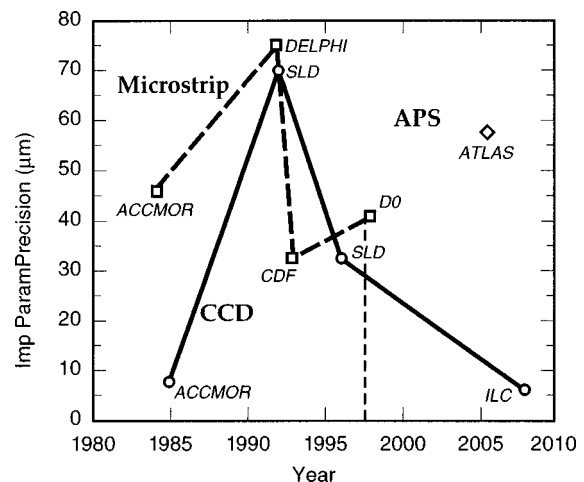


FIG. 30. Multiple scattering term in the formula for impact parameter precision as function of time. For efficient topological reconstruction of heavy flavors including charm, only the very best performance (as measured by this parameter) is adequate.

APS:	active pixel sensor	SV:	secondary vertex (e.g., B decay point)
b, \bar{b} :	beauty/bottom quark, antiquark	T1, T2, T3:	on-CCD transistors
B :	hadron containing b quark	TV:	tertiary vertex (e.g., charm decay following B decay)
BASIS:	base stored image sensor	t, \bar{t} :	top quark, antiquark
BC:	buried channel	V :	vacancy in silicon crystal
BCMD:	bulk charge modulated device	VXD2, VXD3:	initial and upgrade vertex detectors of SLD
CCD:	charge-coupled device	Z^0 :	neutral vector boson
c, \bar{c} :	charm quark, antiquark	$1/f$:	low frequency transistor noise
c.m.:	center-of-mass	c :	speed of light
CDF:	Collide Detector Facility at Fermilab	C_d :	detector capacitance (node-substrate)
CDS:	correlated double sampling	C_g :	gate-source capacitance of first stage output transistor
CMOS:	complementary metal-oxide-semiconductor	C_n :	overall detector node capacitance ($C_d + C_g$)
CMD:	charge modulation device	e^+, e^- :	positron, electron
CTE:	charge transfer efficiency	e^- :	charge on electron
CTI:	charge transfer inefficiency	E :	energy level within silicon crystal
ENC:	equivalent noise charge	E_f :	Fermi energy level
ERF:	extended row filter	E_c :	energy level of conduction band edge
FET:	field effect transistor	E_{tr} :	energy level of trap
HDTV:	high definition television	E_v :	energy level of valence band edge
HEP:	high energy physics	F :	Fano factor
I:	imaging region register, gates, etc. or interstitial silicon atom	f_c :	pixel clocking frequency
IC:	integrated circuit	F_j :	fill factor for trapping under CCD phase j ($j = 1 \dots N_F$)
IERF:	improved extended row filter	H:	horizontal dimension
ILC:	International e^+e^- Linear Collider (future)	I_D :	drain current
IP:	interaction point (i.e., primary vertex)	k :	Boltzmann constant
IR:	interaction region	N_c :	effective density of states in conduction band
$I\phi$:	imaging register gates	N_e :	signal size (number of electrons)
K:	temperature (kelvin)	N_F :	number of phases of CCD register per pixel
K, L, M, \dots :	atomic electron shells	N_s :	signal charge density
LEP:	Large Electron Positron collider at CERN	N_{tr} :	bulk trap density
LHC:	Large Hadron Collider at CERN	P :	particle momentum
MIP:	minimum-ionizing particle	T :	absolute temperature
MNOS:	metal-nitride-oxide-semiconductor	V :	vertical dimension
MOS:	metal-oxide-semiconductor	V_{DD} :	drain-substrate voltage
MOSFET:	metal-oxide-silicon field effect transistor	V_{DS} :	drain-source voltage
n :	neutron	v_n :	electron thermal velocity
NA32:	CERN experiment in the early '80s	V_{FB} :	flat-band voltage
NIEL:	nonionizing energy loss	V_{RD} :	reset voltage
n^-, n, n^+ :	lightly, moderately, heavily doped n -type material	ΔV_{FB} :	change in flat-band voltage
p :	proton	X_n :	entropy factor for bulk trapping
PV:	primary vertex (i.e., interaction point)	W :	mean electron-hole pair creation energy
p^-, p, p^+ :	lightly, moderately, heavily doped p -type material	W_F :	channel width (of output FET)
QC:	quality control	X_0 :	radiation length
R:	readout register, gates, etc.	Z :	atomic number
$R\phi$:	readout register gates	β :	particle velocity/velocity of light or radioactive (electron emitting) source
SC:	surface channel	γ :	total particle energy/mass
Si- E :	phosphorus-vacancy complex in bulk silicon	σ_n :	cross section for electron capture by a bulk trap
SIT:	static induction transistor	$\sigma_{r\phi}$:	impact parameter resolution in $r\phi$ plane (normal to beam direction)
SLC:	Stanford Linear Collider	σ_{rz} :	impact parameter resolution in rz plane
SLD:	SLAC Large Detector		
SRH:	Shockley-Read-Hall (theory of generation recombination)		
SUSY:	supersymmetry theory of elementary particles		

	(containing beam direction and track direction)
θ :	particle direction (polar angle relative to beam direction)
τ_c :	signal trapping time constant
τ_e :	trap emission time constant
τ_g :	dwell time of signal under gate
τ_r :	clock rise-fall time

- ¹C. F. Powell, P. H. Fowler, and D. H. Perkins, *The Study of Elementary Particles by the Photographic Method* (Pergamon New York, 1959).
- ²C. M. G. Lattes, H. Muirhead, C. F. Powell, and G. P. Occhialini, *Nature* (London) **159**, 694 (1947).
- ³W. S. Boyle and G. E. Smith, *Bell Syst. Tech. J.* **49**, 587 (1970).
- ⁴G. F. Amelio, M. F. Tompsett, and G. E. Smith, *Bell Syst. Tech. J.* **49**, 593 (1970).
- ⁵G. Charpak, *Proceedings of the EPS Conference on High Energy Physics, Palermo, 1975*, p. 1291.
- ⁶G. K. McKay, *Phys. Rev.* **84**, 829 (1951).
- ⁷J. Kemmer, *Nucl. Instrum. Methods* **169**, 499 (1980).
- ⁸G. Gilder, *Microcosm: The Quantum Revolution in Economics and Technology* (Touchstone, 1989).
- ⁹C. S. J. Damerell *et al.*, *Nucl. Instrum. Methods Phys. Res.* **185**, 33 (1981).
- ¹⁰R. Bailey *et al.*, *Nucl. Instrum. Methods Phys. Res.* **213**, 201 (1983).
- ¹¹ACCMOR collaboration, *Phys. Lett. B* **236**, 495 (1990).
- ¹²H. Bichsel and R. P. Saxon, *Phys. Rev. A* **11**, 1286 (1975).
- ¹³G. Hall, *Nucl. Instrum. Methods Phys. Res.* **220**, 356 (1984).
- ¹⁴H. Bichsel, *Nucl. Instrum. Methods Phys. Res. A* **235**, 174 (1985).
- ¹⁵H. Bichsel, *Rev. Mod. Phys.* **60**, 663 (1988).
- ¹⁶H. Bichsel, *Nucl. Instrum. Methods Phys. Res. B* **52**, 136 (1990).
- ¹⁷P. Lechner *et al.*, *Nucl. Instrum. Methods Phys. Res. A* **377**, 206 (1996).
- ¹⁸G. W. Fraser *et al.*, *Nucl. Instrum. Methods Phys. Res. A* **350**, 368 (1994).
- ¹⁹J. R. Hauser and P. M. Dunbar, *Solid-State Electron.* **18**, 715 (1975).
- ²⁰C. H. Sequin and M. F. Tompsett, *Charge Transfer Devices* (Academic, New York, 1975).
- ²¹*Charge-Coupled Devices and Systems*, edited by M. J. Howes and D. V. Morgan (Wiley, New York, 1979).
- ²²J. D. E. Beynon and D. R. Lamb, *Charge-Coupled Devices and Their Applications* (McGraw-Hill, New York, 1980).
- ²³C. J. S. Damerell, *Vertex Detectors: The State of the Art and Future Prospects*, Rutherford Lab Preprint RAL-P-95-008 (1995).
- ²⁴G. F. Amelio, W. J. Bertram, and M. F. Tompsett, *IEEE Trans. Electron Devices* **ED-18**, 986 (1971).
- ²⁵R. H. Walden *et al.*, *Bell Syst. Tech. J.* **51**, 1635 (1972).
- ²⁶W. H. Kent, *Bell Syst. Tech. J.* **52**, 1009 (1973).
- ²⁷D. F. Barbe, *Proc. IEEE* **63**, 38 (1975).
- ²⁸T. I. Kamins and G. T. Fong, *IEEE Trans. Electron Devices* **ED-25**, 154 (1978).
- ²⁹N. S. Saks, *IEEE Electron Device Lett.* **EDL-1**, 131 (1980).
- ³⁰H.-Y. Tsoi *et al.*, *IEEE Trans. Electron Devices* **ED-32**, 1525 (1985).
- ³¹D. J. Burt, *Nucl. Instrum. Methods Phys. Res. A* **305**, 564 (1991).
- ³²*IEEE Trans. Electron Devices* **38** (1991) (entire issue).
- ³³D. J. Burt, *GEC J. Res.* **12** (1995).
- ³⁴M. H. White *et al.*, *IEEE J. Solid-State Circuits* **SC-9**, 1 (1974).
- ³⁵J. R. Janesick *et al.*, *IEEE Trans. Nucl. Sci.* **NS-32**, 409 (1985).
- ³⁶G. R. Hopkinson, *Nucl. Instrum. Methods Phys. Res.* **216**, 423 (1983).
- ³⁷G. R. Hopkinson, *Nucl. Instrum. Methods Phys. Res.* **216**, 431 (1983).
- ³⁸A. D. Holland, *Nucl. Instrum. Methods Phys. Res. A* **337**, 334 (1996).
- ³⁹L. J. M. Esser, *Electron. Lett.* **8**, 620 (1972).
- ⁴⁰M. Lax, *J. Phys. Chem. Solids* **8**, 66 (1959).
- ⁴¹J. E. Carnes, W. F. Kosonocky, and E. G. Ramberg, *IEEE J. Solid-State Circuits* **SC-6**, 322 (1971).
- ⁴²J. E. Carnes, W. F. Kosonocky, and E. G. Ramberg, *IEEE Trans. Electron Devices* **ED-19**, 798 (1972).
- ⁴³A. M. Mohsen and M. F. Tompsett, *IEEE Trans. Electron Devices* **ED-21**, 701 (1974).
- ⁴⁴W. Shockley and W. T. Read, *Phys. Rev.* **87**, 835 (1952).
- ⁴⁵R. N. Hall, *Phys. Rev.* **87**, 387 (1952).
- ⁴⁶R. W. Brodersen, D. W. Buss, and A. F. Tasch, *IEEE Trans. Electron Devices* **ED-22**, 40 (1975).
- ⁴⁷M. G. Collet, *IEEE Trans. Electron Devices* **ED-23**, 224 (1976).
- ⁴⁸M. D. Jack and R. H. Dyck, *IEEE Trans. Electron Devices* **ED-23**, 228 (1976).
- ⁴⁹M. Kimata *et al.*, *Jpn. J. Appl. Phys., Part 1* **22**, 975 (1983).
- ⁵⁰E. K. Bangart *et al.*, *IEEE Trans. Electron Devices* **38**, 1162 (1991).
- ⁵¹G. J. Yates *et al.*, *Proc. SPIE* **2549**, 172 (1995).
- ⁵²J. Frenkel, *Phys. Rev.* **54**, 647 (1938).
- ⁵³G. R. Hopkinson and D. H. Lumb, *J. Phys. E* **15**, 1214 (1982).
- ⁵⁴V. Radeka, *Annu. Rev. Nucl. Part. Sci.* **38**, 217 (1988).
- ⁵⁵C. J. S. Damerell *et al.*, *IEEE Trans. Nucl. Sci.* **37**, 305 (1990).
- ⁵⁶K. Abe *et al.*, *Nucl. Instrum. Methods* **A400**, 287 (1997).
- ⁵⁷J. E. Carnes and F. W. Kosonocky, *RCA Rev.* **33**, 327 (1972).
- ⁵⁸S. P. Emmons *et al.*, *Naval Research Lab Report AD-A015 365* (1975).
- ⁵⁹R. W. Brodersen and S. P. Emmons, *IEEE Trans. Electron Devices* **ED-23**, 215 (1976).
- ⁶⁰M. Algranati *et al.*, *Nucl. Instrum. Methods* **164**, 615 (1979).
- ⁶¹R. W. Leach and H. Gursky, *Harvard-Smithsonian Center for Astrophysics preprint* 1196 (1979).
- ⁶²J. Wright, *Dept. of Astronomy Cambridge University* (private communication, 1980).
- ⁶³A. Bross, *Nucl. Instrum. Methods Phys. Res.* **201**, 391 (1982).
- ⁶⁴A. H. Bhuiya, *J. Appl. Phys.* **56**, 2362 (1984).
- ⁶⁵M. Bocciaolini *et al.*, *Nucl. Instrum. Methods Phys. Res. A* **240**, 36 (1985).
- ⁶⁶A. D. Bross and D. B. Clegg, *Nucl. Instrum. Methods Phys. Res. A* **247**, 309 (1986).
- ⁶⁷C. Akerlof *et al.*, *Nucl. Instrum. Methods Phys. Res. A* **260**, 80 (1987).
- ⁶⁸C. J. S. Damerell, *Proceedings of Physics In Collision IV, 1984* (Éditions Frontières, Gif-Sur-Yvette, France, 1985), p. 453.
- ⁶⁹C. Bula, *SLAC-R-494* (1997) p. 495.
- ⁷⁰G. D. Agnew *et al.*, *Proceedings of the 26th Conference on High Energy Physics, Dallas, 1992* (World Scientific, Singapore, 1992), Vol. 2, p. 1862.
- ⁷¹See, for example, SLD collaboration, *Stanford Linear Accelerator Center, SLAC-PUB Nos.* 7117, 7170, 7266, 7278 (1996/7).
- ⁷²J. Killiany, *Top. Appl. Phys.* **38**, 147 (1980).
- ⁷³C. P. Chang and K. P. Aubuchon, *Report No. N00173-77-C-0158*, Hughes Aircraft Co. (1978).
- ⁷⁴J. M. Killiany *et al.*, *IEEE Trans. Nucl. Sci.* **NS-21**, 193 (1974).
- ⁷⁵J. M. Killiany, N. S. Saks, and W. D. Baker, *IEEE Trans. Nucl. Sci.* **NS-22**, 2634 (1975).
- ⁷⁶R. A. Williams and R. D. Nelson, *IEEE Trans. Nucl. Sci.* **NS-22**, 2639 (1975).
- ⁷⁷C. P. Chang, *IEEE Trans. Nucl. Sci.* **NS-24**, 2190 (1977).
- ⁷⁸C. P. Chang, *IEEE Trans. Nucl. Sci.* **NS-25**, 1454 (1978).
- ⁷⁹J. M. Killiany, *IEEE Trans. Compon., Hybrids, Manuf. Technol.* **CHMT-1**, 353 (1978).
- ⁸⁰N. S. Saks *et al.*, *IEEE Trans. Nucl. Sci.* **NS-26**, 5074 (1979).
- ⁸¹N. S. Saks, *IEEE Trans. Nucl. Sci.* **NS-27**, 1727 (1980).
- ⁸²M. S. Robbins, *Ph.D. thesis*, Brunel University, UK, 1992.
- ⁸³E. A. Burke, *IEEE Trans. Nucl. Sci.* **NS-33**, 1276 (1986).
- ⁸⁴G. P. Summers *et al.*, *IEEE Trans. Nucl. Sci.* **NS-33**, 1282 (1986).
- ⁸⁵S. Watts, A. Holmes-Siedle, and A. Holland, *ESA Report BRUCRD-ESACCD-95-IR* (1995).
- ⁸⁶N. S. Saks, *IEEE Trans. Nucl. Sci.* **NS-24**, 2153 (1977).
- ⁸⁷J. R. Srouf, R. A. Hartmann, and S. Othmer, *IEEE Trans. Nucl. Sci.* **NS-27**, 1402 (1980).
- ⁸⁸P. M. Salomon, *Proc. SPIE* **203**, 130 (1979).
- ⁸⁹K. H. Schmidt *et al.*, *Nucl. Instrum. Methods Phys. Res. A* **359**, 634 (1995).
- ⁹⁰J. Janesick *et al.*, *Proc. SPIE* **1447**, 87 (1991).
- ⁹¹A. Holland, A. Abbey, and K. McCarthy, *Proc. SPIE* **1344**, 378 (1990).
- ⁹²M. Kleefstra, *Solid-State Electron.* **21**, 1005 (1978).
- ⁹³L. Strüder *et al.*, *Nucl. Instrum. Methods Phys. Res. A* **257**, 594 (1987).
- ⁹⁴H. Soltau *et al.*, *Nucl. Instrum. Methods Phys. Res. A* **377**, 340 (1996).
- ⁹⁵R. J. Brewer, *IEEE Trans. Nucl. Sci.* **NS-27**, 401 (1980).
- ⁹⁶Y. Matsunaga, H. Yamashita, and S. Ohsawa, *IEEE J. Solid-State Circuits* **26**, 652 (1991).
- ⁹⁷F. Capasso, *Science* **235**, 172 (1987).
- ⁹⁸R. E. Colbeth *et al.*, *Proc. SPIE* **1071**, 108 (1989).
- ⁹⁹E. R. Fossum, *Proc. SPIE* **1900**, 2 (1993).
- ¹⁰⁰O. Yadid-Pecht, R. Ginosar, and Y. Diamand, *IEEE Trans. Electron Devices* **38**, 1772 (1991).
- ¹⁰¹M. Ogata *et al.*, *IEEE Trans. Electron Devices* **37**, 964 (1990).

- ¹⁰²J. Hynecek, IEEE Trans. Electron Devices **38**, 1011 (1991).
- ¹⁰³N. Tanaka, T. Ohmi, and Y. Nakamura, IEEE Trans. Electron Devices **36**, 31 (1989).
- ¹⁰⁴J. Nisizawa, T. Tamamushi, and T. Ohmi, IEEE Trans. Electron Devices **26**, 1970 (1979).
- ¹⁰⁵S. K. Mendis *et al.*, Proc. SPIE **2172**, 19 (1994).
- ¹⁰⁶G. A. Sokol and V. A. E. Shubin, Bull. Lebedev Phys. Inst. **7**, 3 (1991).
- ¹⁰⁷H. Komobuchi and T. Ando, IEEE Trans. Electron Devices **37**, 1861 (1990).
- ¹⁰⁸C. J. Kenney *et al.*, Nucl. Instrum. Methods Phys. Res. A **342**, 59 (1994).
- ¹⁰⁹P. Middelkamp *et al.*, Nucl. Instrum. Methods Phys. Res. A **377**, 532 (1996).
- ¹¹⁰K. H. Becks *et al.*, Nucl. Instrum. Methods Phys. Res. A **386**, 11 (1997).
- ¹¹¹ATLAS inner detector technical design reports CERN/LHCC/97-16 and CERN/LHCC/97-17 (1997).
- ¹¹²CMS technical proposal CERN/LHCC/94-38 (1994).
- ¹¹³F. Abe *et al.*, Phys. Rev. Lett. **74**, 2626 (1995).
- ¹¹⁴C. J. S. Damerell and D. Jackson, New Directions for High Energy Physics: Snowmass 96, Stanford Linear Accelerator Center (1997), p. 442.
- ¹¹⁵S. Hertzbach *et al.*, in Ref. 114, p. 178.